Journal Pre-proofs

Morphological and functional differences between hippocampal and cortical microglia and its impact on neuronal over-excitation in a germline *Pten* mutant mouse model

Zhibing Tan, Parker L. Bussies, Nicholas B. Sarn, Muhammad Irfan, Tara DeSilva, Charis Eng

Please cite this article as: Z. Tan, P.L. Bussies, N.B. Sarn, M. Irfan, T. DeSilva, C. Eng, Morphological and functional differences between hippocampal and cortical microglia and its impact on neuronal over-excitation in a germline *Pten* mutant mouse model, *Neuroscience* (2025), doi: https://doi.org/10.1016/j.neuroscience.2025.02.044

This is a PDF file of an article that has undergone enhancements after acceptance, such as the addition of a cover page and metadata, and formatting for readability, but it is not yet the definitive version of record. This version will undergo additional copyediting, typesetting and review before it is published in its final form, but we are providing this version to give early visibility of the article. Please note that, during the production process, errors may be discovered which could affect the content, and all legal disclaimers that apply to the journal pertain.
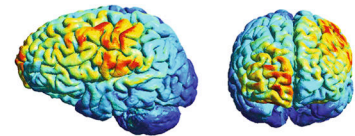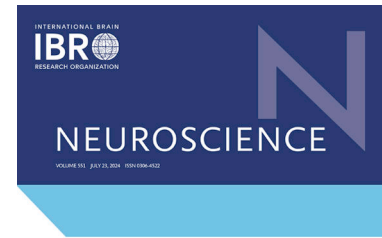
1 **Morphological and functional differences between hippocampal and cortical microglia**
2 **and its impact on neuronal over-excitation in a germline *Pten* mutant mouse model**

3

4 Zhibing Tan[1,2], Parker L. Bussies[1], Nicholas B. Sarn[1], Muhammad Irfan[3], Tara DeSilva[2,3], Charis
5 Eng[1,2,4,5,6,7]

6

7 [1]Genomic Medicine Institute, Lerner Research Institute, Cleveland Clinic, Cleveland, OH 44195,
8 USA; [2]Cleveland Clinic Lerner College of Medicine, Case Western Reserve University, Cleveland,
9 OH 44106, USA; [3]Department of Neurosciences, Lerner Research Institute, Cleveland Clinic,
10 Cleveland, OH 44195, USA; [4]Center for Personalized Genetic Healthcare, Medical Specialties
11 Institute, Cleveland Clinic, Cleveland, OH 44195, USA; [5]Taussig Cancer Institute, Cleveland Clinic,
12 Cleveland, OH 44195, USA; [6]Department of Genetics and Genome Sciences, Case Western
13 Reserve University, Cleveland, OH 44106, USA; [7]Comprehensive Cancer Center, Case Western
14 Reserve University, Cleveland, OH 44106, USA

15

16 **Correspondence to**: Zhibing Tan, MD, PhD, Genomic Medicine Institute, Cleveland Clinic,
17 Lerner Research Institute, 9500 Euclid Avenue, Cleveland, OH 44195, Email: tanz2@ccf.org;
18 Tel: 216 444-0065

1   **Abstract**

2   High-throughput, transcriptomic analyses of the brain have revealed significant differences of
3   microglia between the hippocampus and the cortex. However, it remains unclear whether these
4   regional differences translate into different microglial behaviors and impact disease progression.
5   Here, we show that microglia possess higher morphological complexity and phagocytic capacity
6   in the hippocampus compared to the cortex of wild-type mice. These regional differences are
7   preserved in mice harboring a germline *Pten* mutation, which have a general increase of
8   microglial ramification and phagocytic capacity. Moreover, we find that *Pten*-mutant microglia
9   protect neurons from over-excitation through pruning excessive excitatory synapses and
10 forming more microglia-neuron junctions. However, *Pten*-mutation induced neuronal over-
11 excitation is normalized in the hippocampus but not the cortex which we are attributing to
12 regional differences of microglia in both function and morphology. These *Pten*-mutant microglia
13 may protect *Pten* mutant mice from developing spontaneous seizures, but cannot eliminate their
14 heightened risk of provoked seizure. Collectively, our findings have revealed a potential
15 protective role of microglia in an over-excited brain, underscoring the impact of microglial
16 regional heterogeneity in disease development and highlighting their prospect as a therapeutic
17 target for epilepsy.

18

1 Introduction

2 Microglia, the resident immune cells in the brain, play critical roles in mediating
3 neuroinflammation, regulating neuronal development, and maintaining the homeostasis of the
4 central nervous system (CNS) (Wolf et al., 2017; Li and Barres, 2018; Patel et al., 2019;
5 Umpierre and Wu, 2021). Their phagocytic activities are essential in refining the neuronal
6 circuits of the brain, providing an important mechanism ensuring optimal brain structural and
7 functional plasticity (Kettenmann et al., 2011; Wolf et al., 2017; Tan et al., 2020; Zhao et al.,
8 2024). Microglia undergo dynamic changes at the cellular, subcellular, and molecular level to
9 function within an ever-changing environment. This gives rise to significant phenotypic
10 heterogeneity, such as temporospatial and gender-specific differences in cellular origin,
11 colonization, density, morphology, and gene expression (Grabert et al., 2016; Hanamsagar et
12 al., 2017; Villa et al., 2018; Masuda et al., 2019; Tan et al., 2020). Recent high-throughput,
13 transcriptomic analyses of the brain have revealed significant gene expression differences of
14 microglia between the hippocampus and the cortex (Lawson et al., 1990; Grabert et al., 2016;
15 Morrison et al., 2017; Masuda et al., 2019). Although the variance in microglial phenotypes
16 suggests diverse functionality, the precise connections between regional microglial
17 heterogeneity and their functional diversity remain elusive. Moreover, the extent to which these
18 variations contribute to the progression of neurological disorders, such as epilepsy, remains
19 unclear.

20 The role of microglia in epilepsy, either alleviating or exacerbating seizure activity,
21 remains uncertain. Epilepsy is a prevalent neurological disorder affecting 65-70 million
22 individuals globally (Gibbs-Shelton et al., 2023). It is characterized by recurrent seizures and
23 can be caused by genetic factors, brain injury, infection, and abnormalities in brain structure
24 (Eyo et al., 2017). Multiple studies have shown that microglia are sensitive to the activity of
25 neurons and rapidly become activated during seizures (Liu et al., 2019; Mo et al., 2019;
26 Kinoshita and Koyama, 2021), indicating an active involvement of microglia in seizure activity.
27 Previous studies of epilepsy have reported positive correlations between microglia number and
28 seizure susceptibility during development, as well as seizure mitigation following inhibition of
29 microglial proliferation (Kim et al., 2015; Di Nunzio et al., 2021). However, others have shown
30 microglia to form specialized microglia-neuron junctions to dampen neuronal activity (Li et al.,
31 2012; Kato et al., 2016; Cserep et al., 2020; Merlini et al., 2021). Pharmacological and
32 pharmacogenetic approaches of eliminating microglia have also been shown to increase seizure
33 susceptibility (Wu et al., 2020; Gibbs-Shelton et al., 2023). The discrepancy in observations
34 across studies likely reflects the complex and dynamic role of microglia in regulating seizure.
35 Therefore, an alternative study design is needed to fully understand this relationship, as
36 pharmacological elimination of microglia poses limitations due to its significant disruption of
37 microglial structure, cellular irregularities, cytokine release, and heightened glial reactivity
38 (Rubino et al., 2018; Bedolla et al., 2022). Utilizing genetically modified mouse models holds
39 promise in circumventing these drawbacks and potentially enabling a more precise and
40 accurate phenotyping of microglia.

41 Phosphatase and tensin homolog deleted on chromosome ten (*PTEN*) is an essential
42 regulator of microglia function in the CNS *(Tilot et al., 2016; Sarn et al., 2021b; Sarn et al.,*
43 *2021a)*, an observation which was originally demonstrated by us and has subsequently been
44 replicated by other group (Zhou et al., 2022). PTEN as a well-recognized tumor suppressor
45 gene (Yehia et al., 2020), its germline mutation defines the molecular diagnosis of PTEN
46 Hamartoma Tumor Syndrome (PHTS), which manifests as a wide array of clinical features,
47 including (but not limited to) benign and malignant tumors, autism spectrum disorder (ASD), and
48 epilepsy (Winden et al., 2018). PTEN is expressed in nearly all tissues and works to inhibit the

PI3K/AKT/mTOR signaling pathway, which is important in regulating cell growth, survival, migration, and proliferation (Winden et al., 2018; Yehia et al., 2020). Studies from patients and animal models have shown that *PTEN* mutations in neurons can increase neuronal excitability and reduce seizure threshold (LaSarge et al., 2021; Tariq et al., 2022). These findings have been attributed to *PTEN* mutation-induced overgrowth of dendrites and spines, as well as mutation-induced alterations of potassium channels (Nguyen and Anderson, 2018; LaSarge et al., 2021; Tariq et al., 2022). The function of *Pten* in microglia is characterized by an increase in phagocytic properties and a mutation-dependent change in microglia ramification (hyper- vs hypo-ramified) (Tilot et al., 2016; Sarn et al., 2021b; Zhou et al., 2022). Therefore, in a germline *Pten* mutant model, we anticipated observing both heightened neuronal excitation and morphologically complex/functionally enhanced microglia, which would make for an ideal model to investigate the interactions between microglia and neurons and their contributions to the pathogenesis of epilepsy.

Here, we report microglial differences in morphology and phagocytic capacity between the hippocampus and the cortex. In a heterozygous germline *Pten* mutant mouse model (*Pten^{m3m4/+}*), we find microglia play a beneficial role in mitigating seizure through pruning excessive excitatory synapses and forming more microglia-neuron junctions. These changes proved protective in that they reduced hippocampal neuron excitability from a hyperexcitable state to a more balanced level. Nevertheless, our *Pten^{m3m4/+}* mice harbored an increased susceptibility to seizures, which we attribute to differences in microglial morphology and phagocytic capacity between hippocampus and cortex. Overall, our study reveals novel insights into microglia-neuron interactions, and identifies microglia as an important potential therapeutic target for epilepsy.

Materials and Methods

Animals. Generation of a cytoplasmic-predominant *Pten^{m3m4/m3m4}* mouse model on a CD1 background was previously described by our group (Tilot et al., 2014; Sarn et al., 2021b). The *Pten^{m3m4}* mutation is located within exon 7 of *Pten* and consists of five nucleotide substitution mutations, resulting in four nonsynonymous and one synonymous amino acid changes in the third and fourth putative nuclear localization sequences of *Pten*. Here, we bred mice carrying *Pten^{m3m4}* mutations on a C57/BL6 background. To mimic the situation in PHTS, heterozygote *Pten^{m3m4/+}* mice were compared with wild-type (WT) littermate controls. Confirmatory genotyping was performed on genomic DNA from clipped toes using following PCR primers: WT forward (5′-TGGCAGACTCTTCATTTCTGT GGC-3′), WT reverse (5′-ACTTCTTCACAACCACTT CTTTCAAC-3′), mutant forward (5′-TACCCGGTAGAATTTCGACGACCT-3′), and mutant reverse (5′-ACTTCTTCACAACCACTTCTTTCAAC-3′). Mice were maintained on a 14:10 light-dark cycle with ad libitum access to food and water. Room temperature was maintained between 18 and 26 ℃. Animals were euthanized via CO_2 asphyxiation followed by cervical dislocation. Both male and female mice were used in this project. All experiments were randomized and conducted under protocols approved by the Institutional Animal Care and Use Committee (IACUC) at Cleveland Clinic.

Slice preparation. Mice (P38-43) were anesthetized with isoflurane and subjected to decapitation. Brains were removed rapidly and placed into ice-cold, oxygenated, cutting artificial cerebrospinal fluid (ACSF). The cutting ACSF was composed of the following (in mM): 110 choline Cl, 3.5 KCl, 0.5 $CaCl_2$, 7 $MgCl_2$, 1.3 NaH_2PO_4, 25 $NaHCO_3$, and 20 glucose. After trimming the brain, vibratome (VT1000, Leica) was used to generate 300 μm coronal sections

1 containing both the hippocampus and the cortex. Slices were incubated in oxygenated cutting
2 ACSF at 34 ℃ for 20 minutes, after which they were transferred to fresh normal ACSF at room
3 temperature for at least 40 minutes prior to recording. The normal ACSF used for
4 recovery/recording contained the following (in mM): 125 NaCl, 3.5 KCl, 2 CaCl$_2$, 1.3 MgCl$_2$, 1.3
5 NaH$_2$PO$_4$, 25 NaHCO$_3$, and 10 glucose. All solutions used here were prepared with double
6 distilled water (ddH$_2$O).

7 *Electrophysiology.* Individual slices were transferred to a submerged recording chamber
8 and continuously perfused with the recording ACSF (3.0 ml/min) at 32 ℃. Slices were visualized
9 under infrared video microscopy (Leica DM6000) and differential interference contrast optics.
10 Hippocampal CA1 and cortical layer V pyramidal neurons were identified based on location,
11 shape and size of cell body. Whole-cell patch clamp recordings were made using a MultiClamp
12 700B amplifier, and a 1550B interface (Axon Instruments). Patch electrodes were made from
13 borosilicate glass capillaries (BF150-86-10, Sutter Instruments) with a resistance in the range of
14 2.5-4 MΩ. Action potential (AP) recordings were made using internal solution containing the
15 following (in mM): 125 K-gluconate, 15 KCl, 10 HEPES, 4 MgATP, 0.3 Na$_3$GTP, 0.2 EGTA, and
16 10 phosphocreatine (295 mOsm, pH 7.3, adjusted with KOH). For excitability testing, APs of
17 hippocampal neurons were elicited by injecting step-currents from -25 to 200 pA at the step of
18 25 pA. Likewise, cortical neurons' APs were elicited by injecting step-currents from -50 to 400
19 pA at the step of 50 pA. Intrinsic excitability was examined in the presence of 10 μM bicuculline,
20 20 μM CNQX, and 50 μM DL- AP5 to block synaptic transmission. Post synaptic currents (PSC)
21 were recorded using internal solution containing the following (in mM): 135 CsCH$_3$SO$_3$, 10 CsCl,
22 10 HEPES, 4 MgATP, 0.3 Na$_3$GTP, 5 QX314, 0.2 EGTA, and 10 phosphocreatine (295 mOsm,
23 pH 7.3, adjusted with CsOH). Excitatory PSC (EPSC) and inhibitory PSC (IPSC) were
24 separated by holding the membrane potential at -50 mV (reversal potential of Cl$^-$) and 0 mV
25 (reversal potential of non-selective cation channel), respectively. To record miniature EPSC
26 (mEPSC) and miniature IPSC (mIPSC), 1 μM tetrodotoxin (TTX) was added. To record evoked
27 EPSC (eEPSC), a concentric bipolar electrode (WPI) was placed ~300 μm away from the
28 recorded neurons. Paired-pulse ratio (PPR) was examined by delivering two electrical stimuli at
29 the intervals of 0.025 s, 0.05 s, 0.1 s, 0.2 s, 0.5 s, and 1 s. All signals were filtered at 1 kHz
30 using the amplifier circuitry, sampled at 10 kHz and analyzed using Clampex 11 (Axon
31 Instruments, USA). All solutions used here were prepared with ddH$_2$O.

32 *Microglia phagocytosis assay.* Brain slices were prepared as described above except the
33 slice thickness was reduced to 200 μm to facilitate subsequent immunostaining. Fluorescent
34 beads (Φ=1 μm, L2778, fluorescent red, Sigma-Aldrich) were blocked in fetal bovine serum
35 (FBS, 1:5 v/v) for 1 hour at 37 ℃, after which they were added to normal ACSF to reach a final
36 concentration of 0.02% (v/v). Brain slices were then incubated in the oxygenated ACSF-
37 florescent bead solution for 3 hours at 34 ℃ in a water bath. As only the top side of the slice had
38 full access to the beads during this step (the bottom side was partially blocked by the mesh of
39 the incubating chamber), we only used the top side for downstream evaluation of microglia
40 phagocytosis. Following incubation, slices were washed three times (30 minutes each) with
41 fresh oxygenated ACSF and fixed in 4% PFA overnight. In effort to minimize non-specific bead
42 binding, slices were washed three times (30 minutes each) with phosphate buffered saline
43 (PBS) prior to immunostaining. In ATP-stimulation experiment, ATP and florescent bead were
44 added simultaneously and treated for 3 hours. Because ATP-induced morphological changes in
45 microglia complicated the direct counting of microglia, the averaged-microglial-density from the
46 phagocytosis assay of the same mice without ATP was used to estimate the number of beads
47 ingested per microglia.

1   *Immunohistochemistry and Imaging.* Mice were euthanized via CO2 asphyxiation and
2   perfused transcardially with normal saline (0.9% NaCl) followed by PFA (4%) dissolved in PBS
3   (pH 7.4). Brains were removed and post-fixed in 4% PFA for at least 6 hours, after which they
4   were immersed in 30% sucrose containing PBS until settling. Coronal sections (20 μm) were cut
5   on a cryostat microtome (Leica, UC7) and mounted onto glass slides. The sections were treated
6   with 0.2% Triton X-100 for 30 min and blocked in 10% FBS for 1 hour. Sections were treated
7   with primary antibody diluted in 10% FBS overnight at room temperature. Primary antibodies
8   included Iba1 (1:500, polyclonal, Wako), Kv2.1 (1:200, monoclonal, Antibodiesinc), Gfap (1:500,
9   monoclonal, Santa Cruz), and PV (1:500, monoclonal, Thermo Fisher). After washing off excess
10 primary antibody (PBS, three times, 20 minutes each), sections were incubated with secondary
11 antibody diluted in 10% FBS at room temperature for 2 hours. Secondary antibodies included
12 goat anti-mouse Alexa Fluor 568 (1:1000, Thermo-Fisher) and goat anti-rabbit Alexa Fluor 488
13 (1:1000, Thermo-Fisher). Finally, sections were mounted in Vectashield medium with DAPI
14 (Vector Laboratories) for imaging. To visualize dendritic spines, neurons on live brain slices
15 were patched and back-filled with an internal solution containing 0.1% biocytin. After filling, the
16 slice was fixed overnight by 4% PFA and stained with streptavidin conjugated Alexa-488
17 (1:1,000, Molecular Probes) for 3 days at 4 ℃. For phagocytosis assay, brain slices were
18 stained individually in a 24-well plate, with prolonged incubating time for both primary (3 days)
19 and secondary (1 day) antibodies. In these staining, PBS with 1% Triton X-100 was used for cell
20 permeabilization. Images were acquired using an upright fluorescent microscope (Leica) or an
21 inverted confocal microscope (Leica SP8), as indicated in figure legends. Objective
22 magnification (20X, 63X, or 100X) was selected based on desired image resolution. Serial *z*
23 stack images were taken when structures spanned multiple layers. And in this case, a
24 composite image was generated by projecting at maximum intensity. Images were processed
25 and analyzed using ImageJ2 (also known as Fiji).

26 *Microglia skeleton analysis.* Microglia from the dorsal hippocampus and somatosensory
27 cortex were captured and analyzed. Microglia skeleton morphology was analyzed using
28 ImageJ2 as previously described by Morrison *et al* (Morrison et al., 2017). First, z stack image
29 series were converted to 8-bit and smoothed by the Smooth (3D) plugin. Next, image series
30 were transferred to binary image using the Threshold function of ImageJ2. Image threshold was
31 adjusted to ensure the majority of microglial processes were highlighted. Binary images were
32 skeletonized and analyzed using the Skeletonize (2D/3D) and Analyze Skeleton plugins,
33 respectively.

34 *Seizure induction and behavioral score.* Mice between the ages of P38 and P43 were
35 used in this experiment. Kainic acid (Sigma, 10 mg/ml in normal saline) was injected
36 intraperitoneally (i.p.) to induce epileptic seizures. The dosage used was determined through
37 trial of three dosages (15, 20, and 25mg/kg bodyweight) on a separate cohort of *Pten$^{m3m4/+}$* mice.
38 The 20 mg/kg dose was selected for experimentation because it effectively induced seizure and
39 conferred a low mortality rate. After i.p. injection of kainic acid, mice were placed in a new cage
40 and seizure behavior was observed for 1 hour. At each 10-min interval following injection, the
41 highest level of seizure activity was scored using the following 0-5 Racine's scale system with
42 modifications (Racine, 1972; Sun et al., 2021): (0) free moving, normal behavior; (1) staring and
43 reduced locomotion; (2) head nodding, activation of extensors and rigidity; (3) forelimb clonus
44 and rearing; (4) sustained rearing and falling; (5) loss of posture, tonic seizure, and death.
45 'Latency-to-score 3' was used as a measure of seizure susceptibility and was defined as the
46 time from kainic acid injection to the first score 3 seizure.

47 *Statistics.* Data are presented as mean ± SEM. Statistical comparisons were made using
48 two-way analysis of variance (ANOVA) and paired/unpaired Student's *t*-test as appropriate. For

1　grouped timepoint data, two-way ANOVA with Geisser-Greenhouse correction was used to
2　compare difference between groups. Student's t-test was performed if comparison of individual
3　time point of these grouped data was desired. P values less than 0.05 were considered to be
4　significant.

5

Results

Increased ramification and phagocytic capacity in hippocampal microglia compared to cortical microglia

Recent advances in single-cell RNA sequencing have unveiled considerable spatial and temporal heterogeneity in microglial gene expression across various brain regions, including the hippocampus and cortex (Masuda et al., 2019; Tan et al., 2020). However, the extent to which these genetic variations translate into differences in morphology and function remains an open question. To this end, we performed immunostaining for the microglia marker ionized calcium-binding adapter molecule-1 (Iba1) in brain slices from P40 wild-type (WT) mice and checked the morphology of microglia in the hippocampus and adjacent somatosensory cortex, two major brain regions involved in both ASD and epilepsy (Winden et al., 2018). High-resolution z-stack confocal imaging was employed to capture the detailed morphology of microglia. We found microglia in the hippocampus exhibited greater morphological complexity than those in the cortex (Fig. 1A and B). To quantitatively assess these morphological differences, we performed skeleton analysis of individual microglia. Microglial processes were reliably detected using this method (Supplementary Fig. 1A). Hippocampal microglia were found to possess significantly increased branching and longer processes than those found in the cortex (Fig. 1 C-E). Next, we used Sholl analysis to further validate these findings. We observed a consistent increase in the number of Sholl intersections with respect to the process branching/distance from the soma when comparing hippocampal to cortical microglia (Fig. 1F). Collectively, these data show increased morphological complexity in hippocampal microglia when compared to cortical microglia, with specific increases in ramification and process elongation.

Phagocytosis is one of the major functions of microglia (Li and Barres, 2018; Patel et al., 2019). To determine if the observed morphological difference between hippocampal and cortical microglia correlates with differences in function, we assessed their phagocytic capabilities *in vitro* on brain slices. Acutely prepared live brain slices from P40 WT mice were incubated with 0.02% (v/v) fluorescent beads of 1 μm diameter at 34 ℃ for 3 hours. The slices were subsequently fixed and immunostained for the microglial marker Iba1. Beads co-localizing with Iba1 (Supplementary Fig. 1B) were considered to reflect microglial phagocytosis. As illustrated in Figure 1G and H, we observed that hippocampal microglia exhibited a greater phagocytic capacity for beads compared to cortical microglia, suggesting hippocampal microglia are innately more phagocytic than their cortical counterparts.

Adenosine triphosphate (ATP), a well-characterized microglial chemoattractant and activator, is known to enhance microglial phagocytic activity (Davalos et al., 2005; Dou et al., 2012). To examine whether hippocampal and cortical microglia differ in their response to ATP stimulation, we introduced 10 μM ATP into the bathing solution of our *in vitro* brain slice phagocytosis assay in an independent parallel experiment. As shown in figure 1I and J, ATP augmented phagocytic activity in both hippocampal and cortical microglia, each to a similar extent (hippocampus: 2.66-fold increase, cortex: 2.78-fold increase). When compared directly, hippocampal microglia still phagocyted a greater proportion of beads than cortical microglia (Fig.

1 I and K), indicating that the difference of microglial phagocytosis between hippocampus and cortex persist even under ATP stimulation. Altogether, our findings reveal that hippocampal and cortical microglia differ not only in their morphological characteristics, but also in their phagocytotic propensities.

Increased microglia ramification in both the hippocampus and cortex of *Pten^{m3m4/+}* mice

Pten, the gene implicated in PHTS, is a critical regulator of microglial morphology and function (Sarn et al., 2021b; Sarn et al., 2021a; Vidal-Itriago et al., 2022). All PHTS patients have heterozygous *PTEN* mutations. To this end, we bred our previously described homozygous *Pten^{m3m4/m3m4}* mutant mice with C57BL/6 mice and generated heterozygous mice that carry a single copy of *Pten^{m3m4}* mutation (hereafter referred to as *Pten^{m3m4/+}*) (Tilot et al., 2014; Sarn et al., 2021b). We have previously reported that this particular mutation leads to cytoplasmic predominant mislocalization of Pten, alongside a global reduction in Pten expression across both cytoplasmic and nuclear compartments (Tilot et al., 2014). These effects render it an appropriate model for investigating the functions of Pten. The *Pten^{m3m4/+}* mice exhibited macrocephaly at P40 (Supplementary Fig. 2A and B), akin to human patients with a germline *PTEN* mutation (Yehia et al., 2020). To evaluate the impact of *Pten* mutation on microglia morphology, we conducted Iba1 immunostaining on brain slices from P40 *Pten^{m3m4/+}* mice and their WT littermates. Consistent with our previous report (Sarn et al., 2021b), microglia in the *Pten^{m3m4/+}* mice displayed increased *Iba1* expression, total cell volume, and cell body size (Supplementary Fig. 2C-I), reflecting a status of activation at P40. Images rendered from *z*-stack projection showed that *Pten^{m3m4/+}* microglia were hyper-ramified in the hippocampus and cortex (Fig. 2A), while 3D reconstruction of single microglia corroborated these findings (Fig. 2B). Skeleton analysis of individual microglia showed that *Pten^{m3m4/+}* microglia exhibit increased branching and have longer processes than WT microglia (Fig. 2C-E). Furthermore, Sholl analysis demonstrated that *Pten^{m3m4/+}* microglia have more and longer extension of processes compared to WT microglia in both the hippocampus and cortex (Fig. 2F and 2G). These findings collectively indicate *Pten* plays a crucial role in regulating microglia morphology not only in the cortex, but also in the hippocampus.

Hippocampal microglia exhibit the highest phagocytic capacity, compared to cortical microglia in *Pten^{m3m4/+}* mice

To evaluate whether *Pten* dysfunction alters the regional heterogeneity of microglia morphology within the brain, we analyzed morphology of microglia in the hippocampus and cortex of *Pten^{m3m4/+}* mice. Analysis of the *z*-stack projection images indicated that hippocampal microglia are more hyper-ramified compared to cortical microglia (Fig. 3A). This was supported by 3D reconstruction of individual microglia (Fig. 3B). Quantitative analysis of the microglial skeleton revealed that hippocampal microglia have increased branching and longer processes compared to cortical microglia (Fig. 3C-E). Sholl analysis further confirmed this, showing not only a greater number of microglial processes, but also longer extensions of these processes in hippocampal microglia compared to cortical microglia in *Pten^{m3m4/+}* mice (Fig. 3F). These findings suggest that the morphological differences of microglia, previously noted between the hippocampus and cortex in WT mice, persists in *Pten^{m3m4/+}* mice.

Next, we evaluated phagocytic capacity between hippocampal and cortical microglia populations in *Pten^{m3m4/+}* mice. Following previously established *in vitro* microglia phagocytosis assay, we observed that *Pten^{m3m4/+}* microglia phagocytosed increased number of beads in both the hippocampus and cortex compared to WT (Supplementary Fig. 3A and B), aligning with our previous studies conducted in cultured microglia(Sarn et al., 2021b; Sarn et al., 2021a).

1　Additionally, hippocampal microglia phagocytosed more beads than cortical microglia in
2　*Pten^{m3m4/+}* mice (Fig. 3G and H), indicating heightened phagocytic activity of the hippocampal
3　microglia. These findings suggest that our previously observed difference of WT microglia
4　phagocytic capacity between hippocampus and cortex is maintained in *Pten^{m3m4/+}* mice, with
5　hippocampal microglia possessing an innately higher phagocytic capacity.

6　　　Finally, in an independent experiment, we examined the response of *Pten^{m3m4/+}* microglia
7　to ATP stimulation to determine if there are regional differences between the hippocampus and
8　cortex in ATP-stimulated phagocytosis. We found that ATP-enhanced phagocytosis in cortical
9　microglia but not hippocampal microglia (hippocampus: 1.22-fold increase, cortex: 2.09-fold
10　increase; Fig. 3I and J), implying a unique reaction to ATP stimulation in cortical microglia.
11　Consequently, no significant difference in phagocytic activity was observed between
12　hippocampal and cortical microglia following ATP stimulation in *Pten^{m3m4/+}* mice (Fig. 3I and K).
13　The lack of increased phagocytic activity in hippocampal microglia upon ATP stimulation
14　suggests these microglia may already have reached their peak phagocytic potential as a result
15　of *Pten* mutation. Indeed, further comparison of *Pten^{m3m4/+}* with WT microglia under 10 µM ATP
16　stimulation indicated comparable phagocytic activities in both the hippocampus and cortex
17　(Supplementary Figs. 3C and D). Taken together, these data demonstrate a preserved
18　morphological and phagocytic heterogeneity among hippocampal and cortical microglia in
19　*Pten^{m3m4/+}* mice, as seen in WT mice. Moreover, *Pten* mutation appears to induce region-specific
20　changes in microglial activation, as hippocampal but not cortical microglia reached their ATP-
21　induced peak of phagocytic capacity.

22　**Excitatory synaptic transmission is reduced in the hippocampus but unchanged in the**
23　**cortex of *Pten^{m3m4/+}* mice**

24　*Pten* plays a pivotal role in regulating dendritic spine number, morphology, and plasticity.
25　Numerous studies have shown that neuron-specific *Pten* dysfunction result in dendrite and
26　spine overgrowth (Getz et al., 2022; Tariq et al., 2022). It is well known that microglia are
27　fundamentally involved in synaptic pruning and remodeling (Zhao et al., 2024). In our germline
28　*Pten^{m3m4/+}* mice, we anticipated a concurrent presence of *Pten* mutation-induced spine
29　overgrowth in addition to the observed microglial activation. To understand how these opposing
30　effects integrate within the brain, and to determine whether the microglial morphological and
31　functional differences between the hippocampus and cortex influence the effects of *Pten*
32　mutations on spines, we employed various approaches to assess excitatory synaptic
33　transmission. First, we conducted whole-cell patch-clamp recordings of miniature excitatory
34　postsynaptic current (mEPSC) from CA1 hippocampal pyramidal neurons in the presence of 1
35　µM tetrodotoxin (TTX) and a membrane potential held at -50 mV. The mEPSC events recorded
36　in this condition could be completely blocked by 10 µM AMPA receptor antagonist DNQX and
37　50 µM NMDA receptor antagonist APV (Supplementary Fig. 4A and B), demonstrating the
38　specificity of our recorded events. Comparing mEPSC between WT and *Pten^{m3m4/+}* mice
39　revealed a significant decrease in mEPSC frequency but not amplitude in the hippocampus of
40　the *Pten^{m3m4/+}* mice (Fig. 4A-C). These data suggest that excitatory synaptic transmission is
41　reduced in the hippocampus of *Pten^{m3m4/+}* mice. To discern whether such a reduction was
42　attributable to a decreased probability of synaptic vesicle release versus a reduction in the
43　number of excitatory synapses, we recorded paired-pulse ratio (PPR) of evoked excitatory
44　postsynaptic current (eEPSC) by applying two stimuli at the interval of 0.025 s, 0.05 s, 0.1 s, 0.2
45　s, 0.5 s, and 1 s. The PPR had no significant difference at any of these intervals (Fig. 4D and
46　E), suggesting that the release probability remained unchanged in the hippocampus of
47　*Pten^{m3m4/+}* mice, and that there was an overall reduction in excitatory synaptic numbers. This
48　was further corroborated by directly visualizing dendritic spines through 0.1% biocytin back-

9

1 filling and subsequent Avidin-488 staining of individual CA1 neurons. Spine density calculations,
2 based on the ratio of total spine number to dendritic length, confirmed a significant reduction in
3 spine density in the hippocampus of *Pten^{m3m4/+}* mice compared to WT littermates (Fig. 4F and
4 G). Thus, our findings demonstrate a reduction in the number of excitatory synapses in the
5 hippocampus of germline *Pten* mutant mice at P40.

6 The reduced number of excitatory synapses could be the result of an integrated effect
7 involving neurons, astrocytes, and microglia. To determine if astrocyte abnormalities were
8 present in *Pten^{m3m4/+}* mice, we performed immunostaining for the astrocyte marker glial fibrillary
9 acidic protein (Gfap). We found comparable astrocyte morphology and density between WT and
10 *Pten^{m3m4/+}* mice (Supplementary Fig. 4E and F), suggesting astrocytes are not significantly
11 affected by *Pten* mutation. Further examination of spine density at P14, a critical period of spine
12 formation, revealed a significant increase in spine density in the hippocampus of *Pten^{m3m4/+}* mice
13 compared to WT (Fig. 4H and I). This finding aligns with previous research showing *Pten*
14 dysfunction in neurons leads to an increase in synaptic number (Sarn et al., 2021b; Getz et al.,
15 2022; Tariq et al., 2022). Taken together, these data suggest that the observed hyper-
16 ramified/phagocytic microglia could be playing a crucial role in pruning excess synapses during
17 the development of the hippocampus of our *Pten^{m3m4/+}* mice.

18 Next, we sought to understand how microglial activity affects excitatory synaptic
19 transmission in the cortex of *Pten^{m3m4/+}* mice, given their relatively moderate activation
20 compared to microglia in the hippocampus. First, we conducted whole-cell patch-clamp
21 recording of mEPSC from layer V cortical pyramidal neurons in the presence of 1 μM TTX and a
22 membrane potential held at -50 mV. Both the frequency and amplitude of mEPSC were
23 comparable in the cortex of *Pten^{m3m4/+}* mice and their WT littermates (Fig. 4J-L). These data
24 suggest that excitatory synaptic transmission is not changed in the cortex of *Pten^{m3m4/+}* mice
25 compared to WT. Following this, we evaluated whether the releasing probability of excitatory
26 synapse was altered in the cortex of *Pten^{m3m4/+}* mice. We recorded PPR of eEPSC by applying
27 two stimuli at the intervals of 0.025 s, 0.05 s, 0.1 s, 0.2 s, 0.5 s, and 1 s. PPR had no significant
28 difference at any tested interval (Fig. 4M and N), indicating that the release probability remained
29 unchanged as a result of the *Pten* mutation. Next, we evaluated excitatory synapse number by
30 directly visualizing dendritic spines through 0.1% biocytin back-filling and subsequent Avidin-
31 488 staining. Unlike our investigation of the hippocampus, neuronal spine density was not
32 different between the cortex of *Pten^{m3m4/+}* and WT mice (Fig. 4O and P). Further examination of
33 spine density at P14 mice revealed a significant increase in spine density in the cortex of
34 *Pten^{m3m4/+}* mice compared to WT (Supplementary Fig. 4Q and R), indicating cortical microglia
35 were able to prune excess synapses during the development of *Pten^{m3m4/+}* mice but the extent is
36 slighter compared to hippocampal microglia. In sum, these data imply a differential change of
37 synaptic numbers in the hippocampus and cortex of *Pten^{m3m4/+}* mice compared to WT
38 littermates, potentially attributable to the difference in microglial phagocytic capability between
39 these two brain regions.

40 **Parvalbumin-positive interneuron number is reduced while inhibitory synaptic**
41 **transmission is unchanged in both the hippocampus and cortex of *Pten^{m3m4/+}* mice**

42 Next, we investigated the effects of *Pten* mutation on neuronal inhibitory signaling in the
43 hippocampus and cortex. *Pten* knockout in neurons has been shown to reduce numbers of
44 parvalbumin (PV) and somatostatin (SST) positive interneurons(Vogt et al., 2015). To determine
45 if a similar phenotype exists in our *Pten^{m3m4/+}* mice, we stained brain slices with antibody against
46 interneuron marker PV. We found PV[+] interneuron numbers were significantly reduced at P40 in
47 both the hippocampus and cortex of *Pten^{m3m4/+}* mice when compared to WT littermates (Fig. 5A-

1 C), suggesting impaired PV[+] interneuron development and/or survival in *Pten^m3m4/+* mice. The
2 reduction in PV[+] interneurons was more pronounced in the hippocampus (37.5%) than in the
3 cortex (10%), highlighting regional disparities in the impact of *Pten* mutation on PV[+] interneuron
4 populations. To determine whether the reduction in PV[+] interneurons affects inhibitory synaptic
5 transmission, we recorded miniature inhibitory postsynaptic current (mIPSC) from pyramidal
6 neurons in both hippocampus and layer V cortex using whole-cell patch-clamp. The mIPSC
7 were isolated with 1 μM TTX and the membrane potential held at 0 mV. The specificity of these
8 recordings was confirmed by the complete blockade of mIPSC events with 10 μM bicuculline, a
9 GABA$_A$ receptor antagonist (Supplementary Fig. 4C and D). Surprisingly, we found no
10 significant difference in the frequency or amplitude of mIPSC between *Pten^m3m4/+* and WT mice
11 in either the hippocampus or the cortex (Fig. 5D-I). These data indicate that although PV[+]
12 interneuron numbers are reduced as a result of dysfunctional *Pten* in this model, it does not
13 impact inhibitory synaptic transmission.

14 **Increased cortical but not hippocampal neuronal excitability contributes to the increased**
15 **seizure susceptibility in *Pten^m3m4/+* mice**

16 The *PTEN*-mTOR signaling pathway plays a critical role in regulating neuronal excitability, and
17 *PTEN* mutations have long been associated with increased seizure susceptibility and epilepsy
18 (LaSarge et al., 2021; Cullen et al., 2024). However, only a relatively small portion of PHTS
19 patients (0-14.8%) develop epilepsy (Hansen-Kiss et al., 2017; Shao et al., 2020; Ronzano et
20 al., 2022). This is consistent in our *Pten^m3m4/+* mice, which have not been observed to exhibit
21 spontaneous seizures (data not shown). To explore potential changes in the intrinsic excitability
22 of pyramidal neurons in *Pten^m3m4/+* mice, we recorded step-current injection induced neuronal
23 action potential (AP) firing from both the hippocampus and layer V cortex. To isolate intrinsic
24 excitability from the influence of synaptic transmissions, we added 10 μM DNQX, 50 μM APV,
25 and 10 μM bicuculine in the perfusion solution to block AMPA, NMDA, and GABA receptors,
26 respectively. On average, higher frequency of AP firing was observed in *Pten^m3m4/+* neurons
27 compared to WT littermates (Fig. 6A-D), suggesting an increase in intrinsic excitability in both
28 the hippocampus and cortex of *Pten^m3m4/+* mice. In line with this, the rheobase (which reflects
29 the minimum current required to induce the first AP firing at a 50% probability) was significantly
30 lower in both the hippocampus and cortex of *Pten^m3m4/+* mice (Supplementary Fig. 5A and B).
31 Further investigation confirmed that the resting membrane potential (RMP) and input resistance
32 were similar between *Pten^m3m4/+* and WT neurons (Supplementary Fig. 5C-F), ruling out their
33 potential impact on neuronal excitability. Taken together, we conclude that *Pten* mutation
34 increases neuronal intrinsic excitability regardless of brain regions, consistent with previous
35 studies (LaSarge et al., 2021; Tariq et al., 2022).

36 In general, neuronal excitability is also influenced by excitatory and inhibitory synaptic
37 transmissions. As demonstrated above, inhibitory synaptic transmission was comparable
38 between *Pten^m3m4/+* mice and their WT littermates. However, excitatory synaptic transmission
39 was reduced in the hippocampus but not in the cortex of *Pten^m3m4/+* mice. To investigate the
40 cumulative effect of these synaptic changes on overall neuronal excitability, we recorded step-
41 current injection-induced AP firing with intact synaptic transmissions. In this condition, overall
42 excitability was similar in the hippocampus between *Pten^m3m4/+* and WT mice, but significantly
43 increased in the cortex of *Pten^m3m4/+* mice (Fig. 6E-H). The rheobase mirrored these findings,
44 being reduced in the cortex but similar in the hippocampus of *Pten^m3m4/+* mice (Supplementary
45 Fig. 5G and H), indicating increased excitability of the cortical but not hippocampal neurons in
46 *Pten^m3m4/+* mice. Additionally, we observed no impact of genotype on RMP or input resistance
47 (Supplementary Fig. 5I-L), suggesting little influence of these factors with respect to changes in
48 neuronal excitability. These findings show that the presence of a *Pten* mutation differentially

1 affects overall neuronal excitability in the hippocampus and cortex, and is corelative with the
2 differences observed in microglia between these two regions.

3   Microglia processes are known to form direct junctions with neuronal cell bodies, a
4 phenomenon which is regulated by neuronal activity and believed to protect neuronal function
5 (Li et al., 2012; Kato et al., 2016; Cserep et al., 2020). We explored if *Pten* dysfunction affects
6 the number of microglia-neuron junctions, and whether there are differences between the
7 hippocampus and cortex. Brain slices were co-stained for Iba1 as well as Kv2.1, a voltage-gated
8 potassium channel that anchors vesicle fusion molecules to the neuronal membrane and is
9 implicated in cellular process of cell-to-cell communication (Cserep et al., 2020). Using confocal
10 microscopy, we were able to visualize Kv2.1$^+$ neuronal cell bodies and their interaction with Iba1
11 labeled microglia to identify microglia-neuron junctions (Figure 6I and Supplementary Fig. 5M-
12 O). Z-stack images showed that almost all neuronal cell bodies had direct contact with microglia
13 (Supplementary Fig. 5M-O), an observation that is consistent with previous study (Cserep et al.,
14 2020). However, microglia-neuron junctions in the *Pten^{m3m4/+}* mice seemed to be more abundant
15 due to increased microglial ramification (Supplementary Fig. 5M-O). To better reveal the
16 differences, we analyzed single layer confocal images and quantified the prevalence of these
17 junctions by dividing the number of neurons with junctions to the total number of Kv2.1$^+$
18 neurons. An increased prevalence of microglial contacts was observed in both the hippocampus
19 and cortex of *Pten^{m3m4/+}* mice, though more prominently in the cortex (hippocampus increased
20 by 18.7%, cortex increased by 46.6%, Figure 6I-K). These data suggest that Pten plays a
21 crucial role in governing the quantity of microglia-neuron junctions, and the exist of a positive
22 correlation between the number of microglia-neuron junctions and neuronal excitability.

23   Thus far, we have observed increased intrinsic excitability in both the hippocampus and
24 cortex of *Pten^{m3m4/+}* mice. In the hippocampus, microglia likely normalized overall excitability by
25 reducing the number of excitatory synapses. Conversely, in the cortex, overall excitability was
26 increased due to unchanged excitatory synapses probably because of relatively moderate
27 microglial function. To safeguard neuronal function, more microglia-neuron junctions were
28 formed in the cortex (Fig. 6I-K). These observations suggest that microglia are actively working
29 to protect the brain from over-excitation, and corroborate our finding that *Pten^{m3m4/+}* mice do not
30 exhibit spontaneous seizure. To interrogate this further, we evaluated seizure susceptibility by
31 administering kainic acid, a glutamate receptor agonist, and scored seizure behavior using the
32 revised 0-5 Racine's scale system (Racine, 1972; Sun et al., 2021). More severe seizure
33 behavior was observed in *Pten^{m3m4/+}* mice than in WT littermates (Fig. 6L), with a significantly
34 shorter time to develop severe (score-3) seizures (Fig. 6M). In summary, although *Pten^{m3m4/+}*
35 microglia attempt to modulate neuronal excitability through pruning of excess synapses and
36 formation of specific junctions, *Pten^{m3m4/+}* mice still exhibit increased seizure susceptibility, likely
37 due to microglial heterogeneity across different brain regions.

38

Discussion

40 Microglia's remarkable heterogeneity, evident in varying morphology, gene expression, and
41 functional state, reflects their versatility and adaptability across different brain regions and
42 conditions (Grabert et al., 2016; Wolf et al., 2017; Masuda et al., 2019; Tan et al., 2020). In this
43 study, we demonstrate that hippocampal microglia, compared to cortical microglia, are not only
44 hyper-ramified in morphology but also possess greater phagocytic capabilities. In germline
45 *Pten^{m3m4/+}* mice, we observed a general increase in morphological complexity and phagocytic
46 capability of microglia compared to WT, with these enhancements being more pronounced in

the hippocampal microglia than in the cortical microglia (Fig. 3 and supplementary Fig. 3). This heterogeneity likely contributes to the differential pruning of excess dendritic spines, which normalized the *Pten*-mutation-induced increase of hippocampal but not cortical pyramidal neuron excitability. Given that neuronal-specific knockout of *Pten* generally causes seizure (Barrows et al., 2017; Santos et al., 2017; LaSarge et al., 2021), our findings explain the lack of spontaneous seizure yet increased seizure susceptibility in germline *Pten*$^{m3m4/+}$ mice.

Our electrophysiological and biocytin-labeling experiments showed reduced excitatory synapses in the hippocampus but no change in the cortex of *Pten*$^{m3m4/+}$ mice at P40 (Fig. 4A-G and 4J-P). We attribute this regional difference to differing microglial phagocytic capacities for the following reasons. Spine density is significantly increased in both the hippocampus and cortex of *Pten*$^{m3m4/+}$ mice compared to WT at P14 (Fig. 4H, I, Q, and R), consistent with previous reports that Pten dysfunction in neurons caused spine overgrowth regardless of age (LaSarge et al., 2021; Tariq et al., 2022). Thus, the synaptic reduction in both regions at P40 is likely due to synaptic pruning during development. Both astrocytes and microglia participate in synaptic pruning, but which one is dominant is debated (Konishi et al., 2022). Our data show similar astrocyte morphology and density between *Pten*$^{m3m4/+}$ mice and WT littermates (Supplementary Fig. 4E and F), suggesting moderate effects of Pten on astrocyte. However, due to the limitation of our germline *Pten*-mutant mouse model, we cannot rule out the contribution of other cell types (eg. astrocyte, neuron *etc.*) to the phenotypes we observed here.

The morphological and phagocytotic differences we observed between hippocampal and cortical microglia reflects the complex interplay between the microenvironments of different brain regions and the microglial functional state. In general, hippocampal pyramidal neurons are more excitable compared to cortical pyramidal neurons, probably due to their smaller cell body size and higher input resistance (Supplementary Fig. 5D, F, J, and L) (Tan et al., 2018). The heightened excitation of hippocampal neurons, as well as alterations in various neurotrophic factors, may directly trigger morphological and functional changes and even activation state of hippocampal microglia (Hanamsagar and Bilbo, 2017; Chagas et al., 2020; Umpierre and Wu, 2021). Microglia in a resting homeostatic state tend to be ramified with long, thin processes, while active microglia are more amoeboid in shape (Vidal-Itriago et al., 2022). Between these two states exists an intermediate state where microglia are hyper-ramified and have thicken processes (Streit et al., 1999; Doyle et al., 2017; O'Neil et al., 2018). This state plays a significant role in the brain's response to various stimuli, reflecting a heightened level of alertness and readiness to transition to a fully reactive state if necessary (Davis et al., 2017; Vidal-Itriago et al., 2022). Our findings suggest microglia in the hippocampus are more prone to an intermediate state compared to cortical microglia, because of their increased morphological complexity and phagocytotic capacity. This observation is backed by the genetic findings from current spatial transcriptomic work (Masuda et al., 2019).

Regardless of brain region, *Pten*$^{m3m4/+}$ microglia exhibit increased Iba1 expression, cell volume, cell body size, hyper-ramification, and phagocytotic capacity compared to WT microglia (Fig. 2 and Supplementary Fig.2) (Tilot et al., 2014; Sarn et al., 2021b; Sarn et al., 2021a). These morphological and functional changes are consistent with an intermediate state, suggesting microglia in *Pten*$^{m3m4/+}$ mice are generally hyper-activated. The findings of microglia morphological changes in both germline and microglia-specific *Pten* mutation underpin the influences of genetic background on microglia morphology and function (Sarn et al., 2021b; Sarn et al., 2021a; Zhou et al., 2022). Interestingly, microglia morphological complexity seems correlates with residual of *Pten* functions. Microglia are hypo-ramified in the microglia-specific knockout mice (Zhou et al., 2022), whereas they are hyper-ramified in *Pten* mutant models (Sarn et al., 2021b; Sarn et al., 2021a). This difference could derive from different levels of

residual function of *Pten* in microglia, as well as different functional states of microglia in these mice.

Pten is expressed in almost all cell types of the brain (Endersby and Baker, 2008). Cell type-specific knockout of *Pten* is a commonly used strategy to study the cell-specific role of *Pten* *(LaSarge et al., 2021; Getz et al., 2022; Tariq et al., 2022)*. While this approach isolates the effect of *Pten* in a particular cell type from the influence of other cells, the result can be exaggerated and may not fully reflect the real-life situations, as the majority of patients with PHTS are heterozygous carriers of the *PTEN* gene mutation (Yehia et al., 2020). Our germline *Pten^{m3m4/+}* mouse model closely replicates the observed pathologies of PHTS, providing a consistent genetic background to study the effects of *Pten* gene alterations on disease development. Based on evidence from the literature and our own studies, we believe that both the microglia cell-autonomous and non-autonomous effects of *Pten* contributes to the phenotypes observed in the germline *Pten^{m3m4/+}* mice. *Pten* is expressed in microglia and specific knockout of *Pten* in microglia leads to changes in morphology and increased phagocytotic activity (Zhou et al., 2022). In addition, co-culturing *Pten^{m3m4/m3m4}* microglia with WT neurons reduces synaptic numbers (Sarn et al., 2021b). These findings suggest *Pten^{m3m4}* mutation has cell-autonomous effects on microglial morphology and phagocytotic capacity (Sarn et al., 2021b). Meanwhile, these cell-autonomous influences are further complemented by cell non-autonomous effects of *Pten*. For instance, we previously cultured WT microglia with *Pten^{m3m4/m3m4}* neurons and observed enhanced phagocytosis of synapses (Sarn et al., 2021b), suggesting heightened excitation of neurons directly impact microglial functional states.

It is interesting to find that inhibitory synaptic transmission was unchanged in *Pten^{m3m4/+}* mice (Fig. 5D-I). Similar results were found in the study of a heterozygous *Nkx2.1-Cre^+;Pten^{Flox/+}* mice (Vogt et al., 2015). In that study, the investigators showed PV$^+$ and SST$^+$ interneurons numbers were disproportionally reduced, resulting in an increased PV/SST ratio in the cortex (Vogt et al., 2015). In our germline *Pten^{m3m4/+}* mice, we also found reduced PV$^+$ interneuron numbers in both the hippocampus and cortex (Fig. 5A-C), suggesting Pten signaling is critical for PV$^+$ interneuron development and/or survival. Recent investigation has shown that microglia can also prune inhibitory synapse (Chen et al., 2014; Hashimoto et al., 2023; Haruwaka et al., 2024). It remains unclear how activated microglia selectively prune excess excitatory synapses, and how inhibitory synaptic transmission was unchanged despite an overall reduction of PV$^+$ interneurons. Further studies are needed to determine if there is a compensatory increase in the number of inhibitory synapses formed per interneuron, and/or an increased release probability of inhibitory synapses.

There is considerable data which show microglia play a neuroprotective role by forming specialized junctions between their processes and neuronal cell bodies (Li et al., 2012; Vinet et al., 2012; Cserep et al., 2020). Through these junctions, microglia can monitor the functional state of neurons, respond to changes in neuronal activity or the presence of damage-associated signals, and maintain CNS homeostasis (Li et al., 2012; Vinet et al., 2012; Cserep et al., 2020). We found significantly more microglia-neuron junctions in *Pten^{m3m4/+}* mice than in WT littermates, providing the first evidence that *Pten* can regulate microglia-neuron junction formation. The increase in such junctions could be any combination of increased microglial ramification, elevated neuronal excitation, or simple *Pten* dysfunction in ether cell type. Though microglia-neuron junctions are increased in both the hippocampus and cortex of *Pten^{m3m4/+}* mice, they are more prominent in the cortex (Figure 6I-K), which coincides with increased overall excitability of the cortical neurons but not hippocampal neurons in *Pten^{m3m4/+}* mice. The microglia-neuron junctions were better visualized with superresolution microscopy and transmission electron micrograph (Cserep et al., 2020). The use of confocal imaging in our study limited our ability to

1 calculate the actual numbers of microglia-neuron junctions. Thus, we only compared the
2 prevalence of microglia-neuron junction in this study (Fig. 6I-K).

3 The role of microglia in epilepsy, and whether they serve to alleviate or exacerbate
4 seizure activity, remains uncertain due to the discrepancy in observations across studies (Kim et
5 al., 2015; Gibbs-Shelton et al., 2023). The coexistence of over-excited neurons and
6 morphologically complex/functionally enhanced microglia in the $Pten^{m3m4/+}$ mouse makes it a
7 good model for studying the role of microglia in epilepsy. Our findings suggest $Pten^{m3m4/+}$
8 microglia are protective in epilepsy, as they reduce excitation of pyramidal neurons by pruning
9 excess dendritic spines and forming increased direct junctions with neuronal cell bodies. They
10 are able to fully resolve overexcitation of hippocampal but not cortical neurons, likely due to the
11 differences in microglial morphology and phagocytic capacity between these two brain regions.
12 This may explain the lack of spontaneous seizure, yet increased susceptibility of inducible
13 seizures, in our $Pten^{m3m4/+}$ mice. Clinically, this may also be a reason why only a small portion of
14 the PHTS population develop epilepsy (0-14.8%) and why the majority of these epilepsy are
15 focal (Hansen-Kiss et al., 2017; Shao et al., 2020; Ronzano et al., 2022). Apart from the
16 hippocampus and cortex, the amygdala is another major brain region involved in the
17 pathogenesis of epilepsy. Further studies are needed to investigate how these might contribute
18 to the increased seizure susceptibility of $Pten^{m3m4/+}$ mice.

19 In conclusion, our study reveals significant morphological and functional differences
20 between hippocampal and cortical microglia, which may be augmented as a result of germline
21 $Pten^{m3m4/+}$ mutation. In response to overly-excited neurons, $Pten^{m3m4/+}$ microglia appear to prune
22 an excess of excitatory synapses and to form more neuron-microglia junctions, implying a
23 protective role of $Pten$-mutant microglia in the pathogenesis of epilepsy in the $Pten^{m3m4/+}$ mouse
24 model. It offers novel insights into microglia-neuron interactions and identifies microglia as
25 important in etiopathogenesis of, and hence, potential therapeutic target for the treatment of
26 epilepsy.

27

Acknowledgements

33

Author contributions

35 ZT and CE conceived the idea and wrote the manuscript; ZT carried out the experiments and
36 analyzed the data; PB, NS, MI, and TD edited the manuscript; TD provided reagents and
37 electrophysiological rigs.

38

Competing interests

40 The authors declare no competing interests.

1

2 **Figures and figure legends**

3 **Figure 1.** Morphological and functional differences of microglia between the hippocampus and
4 cortex. (A) Representative *z*-stack confocal images showing the microglial morphology of the
5 WT hippocampus (left) and cortex (right) visualized by Iba1 staining. Scale: 50 μm. (B)
6 Representative 3D reconstruction images showing the microglia morphology in the
7 hippocampus (left) and cortex (right). Scale: 50 μm. (C-E) Summary data showing increased
8 branch end points per cell (C), branch number per cell (D), and process length (E) in
9 hippocampal microglia compared to cortical microglia (n = 8 mice. Branch end points: HPC,
10 102.64 ± 4.5; cortex: 62.52 ± 5.7, $t(14) = 5.535$, P < 0.001. Branch number: HPC: 207.2 ± 11.0;
11 cortex: 125.71 ± 10.5, $t(14) = 5.370$, P < 0.001. Process length: HPC: 0.47 ± 0.02 mm; cortex:
12 0.30 ± 0.02 mm, $t(14) = 5.768$, P < 0.001). (F) Comparison of Sholl analysis of microglia
13 morphology between the hippocampus and cortex ($F(1, 14) = 10.12$, P = 0.0067). (G) Left:
14 representative *z*-stack confocal images showing the Iba1-stained microglia (green) phagocytize
15 fluorescent beads (red); right: processed mask image showing the distribution of phagocyted
16 beads. Please note the dot size does not reflect the real size of the bead because of image
17 processing to make the bead more visible in the image. Scale: 500 μm. (H) Summary data
18 showing average phagocytosis of beads by microglia to be higher in the hippocampus than the
19 cortex (n = 6 mice, HPC: 1.06 ± 0.09 beads/microglia; cortex: 0.56 ± 0.06 beads/microglia,
20 paired *t* test, $t(5) = 4.732$, P = 0.0052). (I) Left: representative *z*-stack confocal images showing
21 ATP increases microglia (green) phagocytic capacity; right: processed mask image showing the
22 distribution of phagocyted beads. Scale: 500 μm. (J) Summary data showing ATP increases
23 microglia phagocytic capacity in both hippocampus and cortex (HPC: control 1.06 ± 0.09
24 beads/microglia; ATP 2.72 ± 0.4, $t(10) = 3.961$, P < 0.01. Cortex: control 0.56 ± 0.06
25 beads/microglia; ATP 1.61 ± 0.1, $t(10) = 6.499$, P < 0.001). (K) Summary data showing average
26 phagocytosis of beads by microglia to be higher in the hippocampus than the cortex when under
27 ATP stimulation (n = 6 mice, HPC: 2.72 ± 0.4 beads/microglia; cortex: 1.61 ± 0.1
28 beads/microglia, paired *t* test, $t(5) = 3.013$, P = 0.03). *P < 0.05, **P < 0.01, ***P < 0.001.
29 Triangle: male, circle: female.

30

31 **Figure 2.** Microglia are hyper-ramified in both the hippocampus and cortex of *Pten*$^{m3m4/+}$ mice.
32 (A) Representative *z*-stack confocal images showing the microglia morphology in the
33 hippocampus (top) and cortex (bottom) of WT (left) and *Pten*$^{m3m4/+}$ mice (right). Scale: 50 μm. (B)
34 Representative 3D reconstruction images showing the microglia morphology in the
35 hippocampus (top) and cortex (bottom) of WT (left) and *Pten*$^{m3m4/+}$ mice (right). Scale: 50 μm.
36 (C-E) Summary data showing increased branch end points per cell (C), branch number per cell
37 (D), and process length (E) in *Pten*$^{m3m4/+}$ microglia compared to WT microglia in both the
38 hippocampus and cortex (n = 8 mice per group. Branch end points: WT HPC, 102.64 ± 4.5,
39 *Pten*$^{m3m4/+}$ HPC, 137.80 ± 8.9, t(14) = 3.529, P = 0.0017; WT cortex, 62.52 ± 5.7, *Pten*$^{m3m4/+}$
40 cortex, 80.15 ± 5.4, $t(14) = 2.247$, P = 0.0413. Branch number: WT HPC: 207.2 ± 11.0,
41 *Pten*$^{m3m4/+}$ HPC: 272.44 ± 20.16, t(14) = 2.841, P < 0.001; WT cortex: 125.71 ± 10.5, *Pten*$^{m3m4/+}$
42 cortex, 159.76 ± 10.6, $t(14) = 2.287$, P = 0.0383. Process length: WT HPC: 0.47 ± 0.02 mm,
43 *Pten*$^{m3m4/+}$ HPC: 0.65 ± 0.04 mm, t(14) = 4.267, P < 0.001; WT cortex: 0.30 ± 0.02 mm,
44 *Pten*$^{m3m4/+}$ HPC: 0.40 ± 0.02 mm, $t(14) = 3.177$, P = 0.0067). (F and G) Comparison of Sholl
45 analysis of microglia morphology between WT and *Pten*$^{m3m4/+}$ in both the hippocampus (F, $F(1,$

1 14) = 20.22, P < 0.001) and cortex (G, F(1, 14) = 5.229, P = 0.0383). *P < 0.05, **P < 0.01, ***P
2 < 0.001. Triangle: male, circle: female.

3

4 **Figure 3.** Morphological and functional differences of microglia between the hippocampus and
5 cortex of $Pten^{m3m4/+}$ mice. (A) Representative z-stack confocal images showing the microglia
6 morphology in the hippocampus (left) and cortex (right) of $Pten^{m3m4/+}$ mice. Scale: 50 μm. (B)
7 Representative 3D reconstruction images showing the microglia morphology in the
8 hippocampus (left) and cortex (right) of $Pten^{m3m4/+}$ mice. Scale: 50 μm. (C-E) Summary data
9 showing increased branch end points per cell (C), branch number per cell (D), and process
10 length (E) in hippocampal microglia compared to cortical microglia of $Pten^{m3m4/+}$ mice (n = 8 mice
11 per group. Branch end points: HPC, 137.80 ± 8.9; cortex: 80.15 ± 5.4, t(14) = 5.54, P < 0.001.
12 Branch number: HPC: 272.44 ± 20.2; cortex: 159.76 ± 10.6, t(14) = 4.947, P < 0.001. Process
13 length: HPC: 0.66 ± 0.04 mm; cortex: 0.4 ± 0.02 mm, t(65) = 1.997, P < 0.001). (F) Comparison
14 of Sholl analysis of microglia morphology between the hippocampus and cortex of $Pten^{m3m4/+}$
15 mice (F(1, 14) = 11.12, P = 0.0049). (G) Left: representative z-stack confocal images showing
16 the Iba1-stained microglia (green) phagocytize fluorescent beads (red); right: processed mask
17 image showing the distribution of phagocytized beads. Scale: 500 μm. (H) Summary data
18 showing average phagocytosis of beads by microglia to be higher in the hippocampus than in
19 the cortex of $Pten^{m3m4/+}$ mice (n = 6 mice, HPC: 1.79 ± 0.2 beads/microglia; cortex: 1.0 ± 0.1
20 beads/microglia, paired t-test, t(5) = 5.4, P = 0.003). (I) Left: representative z-stack confocal
21 images showing ATP increases cortical but not hippocampal microglia (green) phagocytic
22 capacity in $Pten^{m3m4/+}$ mice; right: processed mask image showing the distribution of
23 phagocytized beads. Scale: 500 μm. (J) Summary data showing the effects of ATP on microglia
24 phagocytic capacity in both hippocampus and cortex (HPC: control 1.79 ± 0.2 beads/microglia;
25 ATP HPC: 2.25 ± 0.3, t(10) = 1.3, P = 0.222. Cortex: control 1.0 ± 0.1 beads/microglia; ATP
26 cortex: 2.07 ± 0.2, t(10) = 4.85, P < 0.001). (K) Summary data showing $Pten^{m3m4/+}$ hippocampal
27 microglia phagocytized similar bead amounts as cortical microglia under ATP stimulation (n = 6
28 mice, HPC: 2.25 ± 0.3 beads/microglia; cortex: 2.07 ± 0.2 beads/microglia, paired t test, t(5) =
29 1.147, P = 0.303). *P < 0.05, **P < 0.01, ***P < 0.001. Triangle: male, circle: female.

30

31 **Figure 4.** Excitatory synaptic transmission is reduced in the hippocampus but unchanged in the
32 cortex of $Pten^{m3m4/+}$ mice. (A) Representative traces of mEPSCs recorded from hippocampal
33 pyramidal neurons of WT (top) and $Pten^{m3m4/+}$ mice (bottom). (B and C) Summary data showing
34 reduced mEPSCs frequency (B, n = 10 neurons from 1 male and 2 female mice for each group,
35 WT: 2.27 ± 0.4 Hz, $Pten^{m3m4/+}$: 0.99 ± 0.2 Hz, t(18) = 3.225, P = 0.0047) but not amplitude (C, n
36 = 10 neurons from 1 male and 2 female mice for each group, WT: 16.25 ± 0.5 pA, $Pten^{m3m4/+}$:
37 15.67 ± 0.6 pA, t(18) = 0.742, P = 0.467) in hippocampal pyramidal neurons of $Pten^{m3m4/+}$ mice
38 compared to WT. (D) Representative traces of paired-pulse stimuli at the intervals of 25 ms, 50
39 ms, and 100 ms. Recordings were made from hippocampal pyramidal neurons of WT (top) and
40 $Pten^{m3m4/+}$ mice (bottom). (E) Summary data showing no significant difference in paired-pulse
41 ratio between hippocampal pyramidal neurons of WT and $Pten^{m3m4/+}$ mice (n = 8 neurons from 1
42 male and 2 female mice for each group, F(1, 14) = 0.91, P = 0.357). (F) Representative z-stack
43 confocal images showing dendritic spines of hippocampal pyramidal neurons from P40 WT (top)
44 and $Pten^{m3m4/+}$ mice (bottom). Scale bar: 10 μm. (G) Summary data showing reduced dendritic
45 spine density in $Pten^{m3m4/+}$ mice compared to WT at P40 (WT n = 6 mice, 1.32 ± 0.06 spine/μm;
46 $Pten^{m3m4/+}$ n = 6 mice, 1.13 ± 0.05 spine/μm; t(10) = 2.356, P = 0.04). (H) Representative z-stack

confocal images showing dendritic spines of hippocampal pyramidal neurons from P14 WT (top) and *Pten*^{m3m4/+} mice (bottom). Scale bar: 10 μm. (I) Summary data showing increased hippocampal dendritic spine density in *Pten*^{m3m4/+} mice compared to WT at P14 (WT n = 6 mice, 1.12 ± 0.04 spine/μm; *Pten*^{m3m4/+} n = 6 mice, 1.35 ± 0.06 spine/μm; t(10) = 3.168, P = 0.01). (J) Representative traces of mEPSCs recorded from cortical pyramidal neurons of WT (top) and *Pten*^{m3m4/+} mice (bottom). (K and L) Summary data showing unchanged mEPSC frequency (K, n = 10 neurons from 2 male and 2 female mice for each group, WT: 4.71 ± 0.8 Hz, *Pten*^{m3m4/+}: 7.19 ± 1.1 Hz, t(18) = 1.883, P = 0.076) and amplitude (L, n = 10 neurons from 2 male and 2 female mice, WT: 17.88 ± 0.4 pA, *Pten*^{m3m4/+}: 19.04 ± 0.9 pA, t(18) = 1.149, P = 0.265) in cortical pyramidal neurons of *Pten*^{m3m4/+} mice compared to WT. (M) Representative traces of paired-pulse stimuli at the intervals of 25 ms, 50 ms, and 100 ms. Recordings were made from cortical pyramidal neurons of WT (top) and *Pten*^{m3m4/+} mice (bottom). (N) Summary data showing no significant difference in paired-pulse ratio between cortical pyramidal neurons of WT and *Pten*^{m3m4/+} mice (n = 7 neurons from 2 male and 1 female mice for WT and n = 8 neurons from 1 male and 2 female mice for *Pten*^{m3m4/+}, F(1, 13) = 0.22, P = 0.645). (O) Representative *z*-stack confocal images showing dendritic spines of cortical pyramidal neurons from P40 WT (top) and *Pten*^{m3m4/+} mice (bottom). Scale bar: 10 μm. (P) Summary data showing unchanged cortical dendritic spine density in *Pten*^{m3m4/+} mice compared to WT at P40 (WT n = 6 mice, 0.73 ± 0.07 spine/μm; *Pten*^{m3m4/+} n = 6 mice, 0.82 ± 0.09 spine/μm; t(10) = 0.842, P = 0.419). (Q) Representative *z*-stack confocal images showing dendritic spines of cortical pyramidal neurons from P14 WT (top) and *Pten*^{m3m4/+} mice (bottom). Scale bar: 10 μm. (R) Summary data showing increased cortical dendritic spine density in *Pten*^{m3m4/+} mice compared to WT at P14 (WT n = 6 mice, 0.74 ± 0.04 spine/μm; *Pten*^{m3m4/+} n = 6 mice, 0.9 ± 0.04 spine/μm; t(10) = 2.932, P =0.01). **P < 0.01, ***P < 0.001. Triangle: male, circle: female.

Figure 5. Parvalbumin-positive interneuron numbers are reduced but inhibitory transmission is intact in *Pten*^{m3m4/+} mice. (A) Representative fluorescent microscope images showing reduced PV+ interneuron numbers in the hippocampus (top) and cortex (bottom) of *Pten*^{m3m4/+} mice (right) compared to WT mice (left). Scale: 200 μm. (B and C) Summary data showing reduced PV+ interneuron numbers in the hippocampus (B, WT n = 6 mice, 80.23 ± 4.8 neuron/mm^2; *Pten*^{m3m4/+} n = 6 mice, 50.41 ± 5.1 neuron/mm^2; t(10) = 4.25, P = 0.002) and cortex (C, WT n = 6 mice, 150.78 ± 3.1 neuron/mm^2; *Pten*^{m3m4/+} n = 6 mice, 134.67 ± 6.3 neuron/mm^2; t(10) = 2.3, P = 0.044) of *Pten*^{m3m4/+} mice compared to WT mice. (D) Representative traces of mIPSCs recorded from hippocampal pyramidal neurons of WT (top) and *Pten*^{m3m4/+} mice (bottom). (E and F) Summary data showing comparable mIPSC frequency (E, n = 10 neurons from 2 male and 2 female mice for each group, WT: 6.57 ± 1.0 Hz, *Pten*^{m3m4/+}: 6.90 ± 0.5 Hz, t(18) = 0.3, P = 0.767) and amplitude (F, n = 10 neurons from 2 male and 2 female mice for each group, WT: 22.35 ± 1.2 pA, *Pten*^{m3m4/+}: 25.66 ± 2.0 pA, t(18) = 1.432, P = 0.169) between hippocampal pyramidal neurons of WT and *Pten*^{m3m4/+} mice. (G) Representative traces of mIPSCs recorded from cortical pyramidal neurons of WT (top) and *Pten*^{m3m4/+} mice (bottom). (H and I) Summary data showing comparable mIPSC frequency (H, n = 10 neurons from 2 male and 2 female mice for each group, WT: 13.19 ± 2.0 Hz, *Pten*^{m3m4/+}: 16.96 ± 1.5 Hz, t(18) = 1.489, P = 0.154) and amplitude (I, n = 10 neurons from 2 male and 2 female mice for each group, WT: 26.01 ± 1.7 pA, *Pten*^{m3m4/+}: 29.81 ± 1.9 pA, t(18) = 1.519, P = 0.146) between hippocampal pyramidal neurons of WT and *Pten*^{m3m4/+} mice. *P < 0.05, ***P < 0.001. Triangle: male, circle: female.

Figure 6. Increased seizure susceptibility in $Pten^{m3m4/+}$ mice is led by increased cortical but not hippocampal neuronal excitability. (A) Representative traces of AP firing in the presence of synaptic transmission blockers recorded from hippocampal pyramidal neurons of WT (top) and $Pten^{m3m4/+}$ mice (bottom). (B) Summary data showing increased AP frequency in hippocampal pyramidal neurons of $Pten^{m3m4/+}$ mice compared to WT (n = 8 neurons from 2 male and 1 female mice for WT and n = 9 neurons from 1 male and 2 female mice for $Pten^{m3m4/+}$, $F(1, 15) = 19.25$, $P < 0.001$). (C) Representative traces of AP firing in the presence of synaptic transmission blockers recorded from cortical pyramidal neurons of WT (top) and $Pten^{m3m4/+}$ mice (bottom). (D) Summary data showing increased AP frequency in cortical pyramidal neurons of $Pten^{m3m4/+}$ mice compared to WT (n = 8 neurons from 1 male and 2 female mice for WT and n = 10 neurons from 2 male and 2 female mice for $Pten^{m3m4/+}$, $F(1, 16) = 12.13$, $P = 0.003$). (E) Representative traces of AP firing recorded from hippocampal pyramidal neurons of WT (top) and $Pten^{m3m4/+}$ mice (bottom). (F) Summary data showing unchanged AP frequency in hippocampal pyramidal neurons of $Pten^{m3m4/+}$ mice compared to WT (n = 8 neurons from 2 male and 1 female mice for WT and n = 7 neurons from 1 male and 2 female mice for $Pten^{m3m4/+}$, $F(1, 13) = 0.092$, $P = 0.767$). (G) Representative traces of AP firing recorded from cortical pyramidal neurons of WT (top) and $Pten^{m3m4/+}$ mice (bottom). (H) Summary data showing increased AP frequency in cortical pyramidal neurons of $Pten^{m3m4/+}$ mice compared to WT (n = 7 neurons from 1 male and 2 female mice for WT and n = 6 neurons from 2 male and 1 female mice for $Pten^{m3m4/+}$, $F(1, 11) = 12.95$, $P = 0.004$). (I) Representative confocal images showing increased microglia-neuron junctions in the hippocampus (top) and cortex (bottom) of $Pten^{m3m4/+}$ mice (right) compared to WT mice (left). Zoomed view of white square area is shown right beside each low power image. Scale: 25 μm and 10 μm. (J and K) Summary data showing increased prevalence of microglia-neuron junctions in the hippocampus (J, WT n = 6 mice, $41.65 \pm 2.4\%$; $Pten^{m3m4/+}$ n = 6 mice, $49.21 \pm 1.9\%$; $t(10) = 2.496$, $P = 0.032$) and cortex (K, WT n = 6 mice, $30.24 \pm 1.5\%$; $Pten^{m3m4/+}$ n = 6 mice, $44.1 \pm 1.8\%$; $t(10) = 5.99$, $P < 0.001$) of $Pten^{m3m4/+}$ mice compared to WT mice. (L) Summary data showing increased Racine score of kainic acid-induced seizure in $Pten^{m3m4/+}$ mice compared to WT mice (n = 20 mice for both genotypes, $F(1, 38) = 19.97$, $P < 0.001$). (M) Summary data showing shortened latency to score 3 seizure in $Pten^{m3m4/+}$ mice compared to WT mice (n = 9 mice for WT and n = 16 mice for $Pten^{m3m4/+}$ mice, $t(23) = 4.809$, $P < 0.001$). $*P < 0.05$, $**P < 0.01$, $***P < 0.001$. Triangle: male, circle: female.

References

Barrows CM, McCabe MP, Chen H, Swann JW, Weston MC (2017) PTEN Loss Increases the Connectivity of Fast Synaptic Motifs and Functional Connectivity in a Developing Hippocampal Network. J Neurosci 37:8595-8611.

Bedolla A, Taranov A, Luo F, Wang J, Turcato F, Fugate EM, Greig NH, Lindquist DM, Crone SA, Goto J, Luo Y (2022) Diphtheria toxin induced but not CSF1R inhibitor mediated microglia ablation model leads to the loss of CSF/ventricular spaces in vivo that is independent of cytokine upregulation. J Neuroinflammation 19:3.

Chagas LDS, Sandre PC, Ribeiro ERNCA, Marcondes H, Oliveira Silva P, Savino W, Serfaty CA (2020) Environmental Signals on Microglial Function during Brain Development, Neuroplasticity, and Disease. Int J Mol Sci 21.
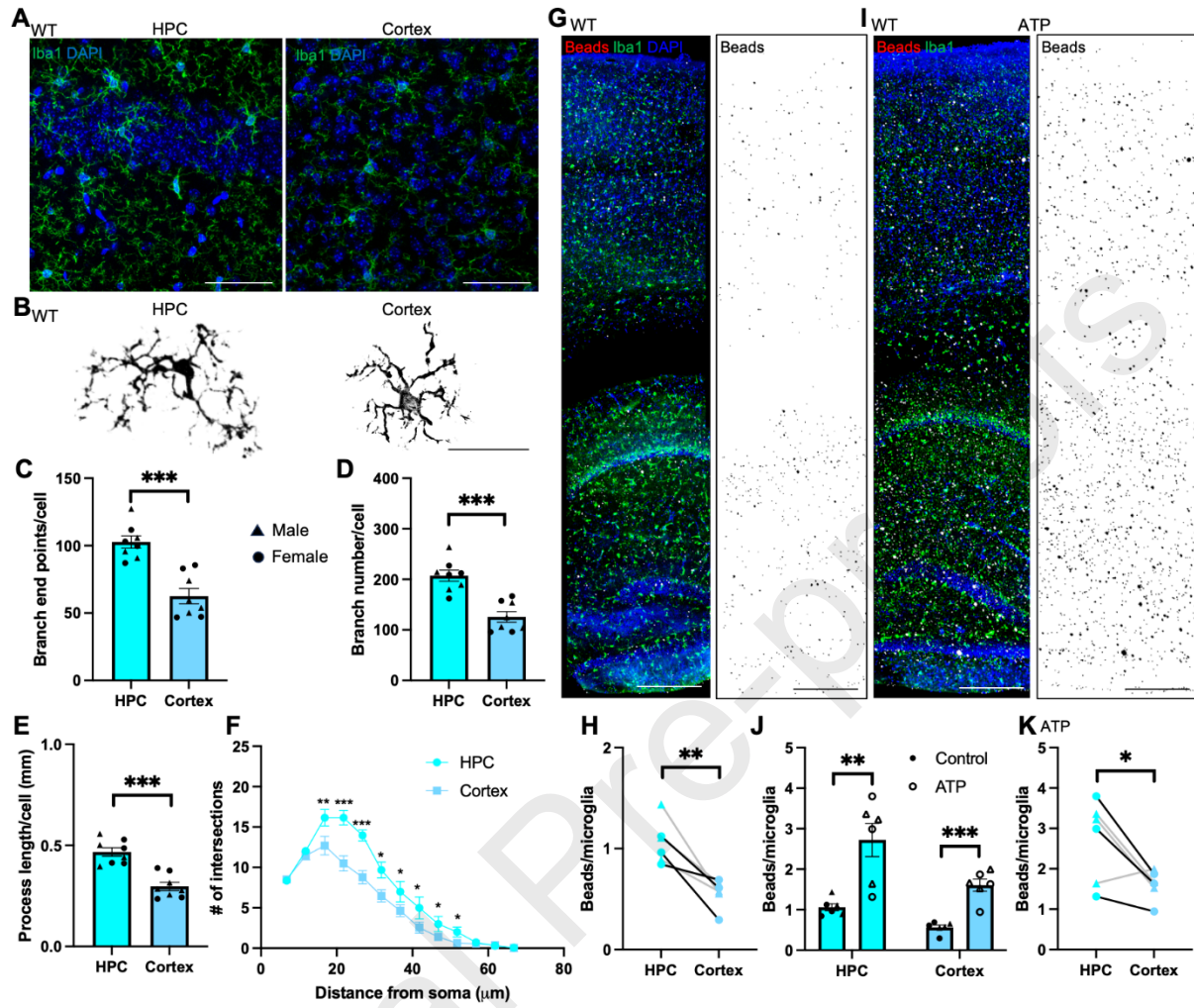
1 Chen Z, Jalabi W, Hu W, Park HJ, Gale JT, Kidd GJ, Bernatowicz R, Gossman ZC, Chen JT, Dutta R, Trapp
2   BD (2014) Microglial displacement of inhibitory synapses provides neuroprotection in the adult
3   brain. Nat Commun 5:4486.

4 Cserep C et al. (2020) Microglia monitor and protect neuronal function through specialized somatic
5   purinergic junctions. Science 367:528-537.

6 Cullen ER, Safari M, Mittelstadt I, Weston MC (2024) Hyperactivity of mTORC1- and mTORC2-dependent
7   signaling mediates epilepsy downstream of somatic PTEN loss. Elife 12.

8 Davalos D, Grutzendler J, Yang G, Kim JV, Zuo Y, Jung S, Littman DR, Dustin ML, Gan WB (2005) ATP
9   mediates rapid microglial response to local brain injury in vivo. Nat Neurosci 8:752-758.

10 Davis BM, Salinas-Navarro M, Cordeiro MF, Moons L, De Groef L (2017) Characterizing microglia
11   activation: a spatial statistics approach to maximize information extraction. Sci Rep 7:1576.

12 Di Nunzio M, Di Sapia R, Sorrentino D, Kebede V, Cerovic M, Gullotta GS, Bacigaluppi M, Audinat E,
13   Marchi N, Ravizza T, Vezzani A (2021) Microglia proliferation plays distinct roles in acquired
14   epilepsy depending on disease stages. Epilepsia 62:1931-1945.

15 Dou Y, Wu HJ, Li HQ, Qin S, Wang YE, Li J, Lou HF, Chen Z, Li XM, Luo QM, Duan S (2012) Microglial
16   migration mediated by ATP-induced ATP release from lysosomes. Cell Res 22:1022-1033.

17 Doyle HH, Eidson LN, Sinkiewicz DM, Murphy AZ (2017) Sex Differences in Microglia Activity within the
18   Periaqueductal Gray of the Rat: A Potential Mechanism Driving the Dimorphic Effects of
19   Morphine. J Neurosci 37:3202-3214.

20 Endersby R, Baker SJ (2008) PTEN signaling in brain: neuropathology and tumorigenesis. Oncogene
21   27:5416-5430.

22 Eyo UB, Murugan M, Wu LJ (2017) Microglia-Neuron Communication in Epilepsy. Glia 65:5-18.

23 Getz SA, Tariq K, Marchand DH, Dickson CR, Howe Vi JR, Skelton PD, Wang W, Li M, Barry JM, Hong J,
24   Luikart BW (2022) PTEN Regulates Dendritic Arborization by Decreasing Microtubule
25   Polymerization Rate. J Neurosci 42:1945-1957.

26 Gibbs-Shelton S, Benderoth J, Gaykema RP, Straub J, Okojie KA, Uweru JO, Lentferink DH, Rajbanshi B,
27   Cowan MN, Patel B, Campos-Salazar AB, Perez-Reyes E, Eyo UB (2023) Microglia play beneficial
28   roles in multiple experimental seizure models. Glia.

29 Grabert K, Michoel T, Karavolos MH, Clohisey S, Baillie JK, Stevens MP, Freeman TC, Summers KM,
30   McColl BW (2016) Microglial brain region-dependent diversity and selective regional sensitivities
31   to aging. Nat Neurosci 19:504-516.

32 Hanamsagar R, Bilbo SD (2017) Environment matters: microglia function and dysfunction in a changing
33   world. Curr Opin Neurobiol 47:146-155.

1   Hanamsagar R, Alter MD, Block CS, Sullivan H, Bolton JL, Bilbo SD (2017) Generation of a microglial
2   developmental index in mice and in humans reveals a sex difference in maturation and immune
3   reactivity. Glia 65:1504-1520.

4   Hansen-Kiss E, Beinkampen S, Adler B, Frazier T, Prior T, Erdman S, Eng C, Herman G (2017) A
5   retrospective chart review of the features of PTEN hamartoma tumour syndrome in children. J
6   Med Genet 54:471-478.

7   Haruwaka K, Ying Y, Liang Y, Umpierre AD, Yi MH, Kremen V, Chen T, Xie T, Qi F, Zhao S, Zheng J, Liu YU,
8   Dong H, Worrell GA, Wu LJ (2024) Microglia enhance post-anesthesia neuronal activity by
9   shielding inhibitory synapses. Nat Neurosci.

10 Hashimoto A, Kawamura N, Tarusawa E, Takeda I, Aoyama Y, Ohno N, Inoue M, Kagamiuchi M, Kato D,
11   Matsumoto M, Hasegawa Y, Nabekura J, Schaefer A, Moorhouse AJ, Yagi T, Wake H (2023)
12   Microglia enable cross-modal plasticity by removing inhibitory synapses. Cell Rep 42:112383.

13 Kato G, Inada H, Wake H, Akiyoshi R, Miyamoto A, Eto K, Ishikawa T, Moorhouse AJ, Strassman AM,
14   Nabekura J (2016) Microglial Contact Prevents Excess Depolarization and Rescues Neurons from
15   Excitotoxicity. eNeuro 3.

16 Kettenmann H, Hanisch UK, Noda M, Verkhratsky A (2011) Physiology of microglia. Physiol Rev 91:461-
17   553.

18 Kim I, Mlsna LM, Yoon S, Le B, Yu S, Xu D, Koh S (2015) A postnatal peak in microglial development in the
19   mouse hippocampus is correlated with heightened sensitivity to seizure triggers. Brain Behav
20   5:e00403.

21 Kinoshita S, Koyama R (2021) Pro- and anti-epileptic roles of microglia. Neural Regen Res 16:1369-1371.

22 Konishi H, Koizumi S, Kiyama H (2022) Phagocytic astrocytes: Emerging from the shadows of microglia.
23   Glia 70:1009-1026.

24 LaSarge CL, Pun RYK, Gu Z, Riccetti MR, Namboodiri DV, Tiwari D, Gross C, Danzer SC (2021) mTOR-
25   driven neural circuit changes initiate an epileptogenic cascade. Prog Neurobiol 200:101974.

26 Lawson LJ, Perry VH, Dri P, Gordon S (1990) Heterogeneity in the distribution and morphology of
27   microglia in the normal adult mouse brain. Neuroscience 39:151-170.

28 Li Q, Barres BA (2018) Microglia and macrophages in brain homeostasis and disease. Nat Rev Immunol
29   18:225-242.

30 Li Y, Du XF, Liu CS, Wen ZL, Du JL (2012) Reciprocal regulation between resting microglial dynamics and
31   neuronal activity in vivo. Dev Cell 23:1189-1202.

32 Liu YU, Ying Y, Li Y, Eyo UB, Chen T, Zheng J, Umpierre AD, Zhu J, Bosco DB, Dong H, Wu LJ (2019)
33   Neuronal network activity controls microglial process surveillance in awake mice via
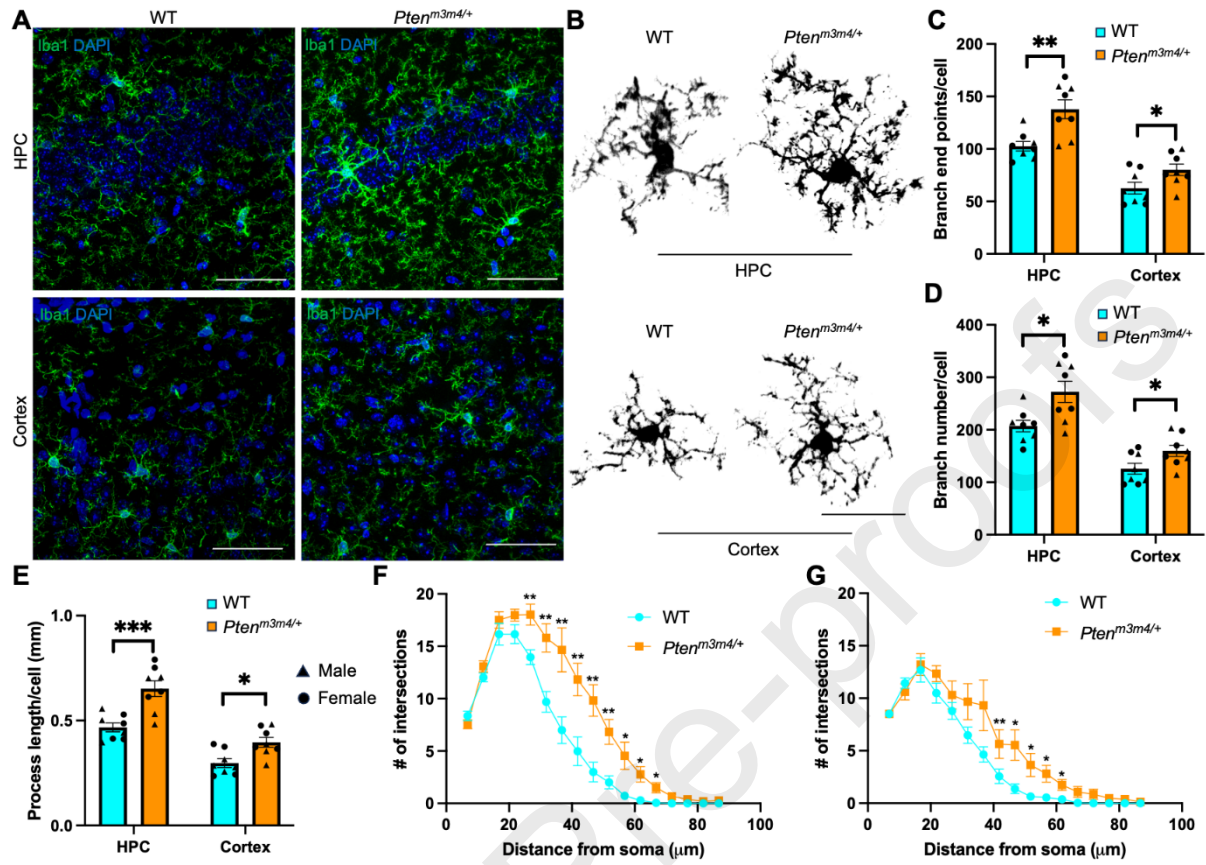34   norepinephrine signaling. Nat Neurosci 22:1771-1781.

1 Masuda T, Sankowski R, Staszewski O, Bottcher C, Amann L, Sagar, Scheiwe C, Nessler S, Kunz P, van Loo
2 G, Coenen VA, Reinacher PC, Michel A, Sure U, Gold R, Grun D, Priller J, Stadelmann C, Prinz M
3 (2019) Spatial and temporal heterogeneity of mouse and human microglia at single-cell
4 resolution. Nature 566:388-392.

5 Merlini M et al. (2021) Microglial G(i)-dependent dynamics regulate brain network hyperexcitability. Nat
6 Neurosci 24:19-23.

7 Mo M, Eyo UB, Xie M, Peng J, Bosco DB, Umpierre AD, Zhu X, Tian DS, Xu P, Wu LJ (2019) Microglial
8 P2Y12 Receptor Regulates Seizure-Induced Neurogenesis and Immature Neuronal Projections. J
9 Neurosci 39:9453-9464.

10 Morrison H, Young K, Qureshi M, Rowe RK, Lifshitz J (2017) Quantitative microglia analyses reveal
11 diverse morphologic responses in the rat cortex after diffuse brain injury. Sci Rep 7:13211.

12 Nguyen LH, Anderson AE (2018) mTOR-dependent alterations of Kv1.1 subunit expression in the
13 neuronal subset-specific Pten knockout mouse model of cortical dysplasia with epilepsy. Sci Rep
14 8:3568.

15 O'Neil SM, Witcher KG, McKim DB, Godbout JP (2018) Forced turnover of aged microglia induces an
16 intermediate phenotype but does not rebalance CNS environmental cues driving priming to
17 immune challenge. Acta Neuropathol Commun 6:129.

18 Patel DC, Tewari BP, Chaunsali L, Sontheimer H (2019) Neuron-glia interactions in the pathophysiology
19 of epilepsy. Nat Rev Neurosci 20:282-297.

20 Racine RJ (1972) Modification of seizure activity by electrical stimulation. II. Motor seizure.
21 Electroencephalogr Clin Neurophysiol 32:281-294.

22 Ronzano N, Scala M, Abiusi E, Contaldo I, Leoni C, Vari MS, Pisano T, Battaglia D, Genuardi M, Elia M,
23 Striano P, Pruna D (2022) Phosphatase and tensin homolog (PTEN) variants and epilepsy: A
24 multicenter case series. Seizure 100:82-86.

25 Rubino SJ, Mayo L, Wimmer I, Siedler V, Brunner F, Hametner S, Madi A, Lanser A, Moreira T, Donnelly
26 D, Cox L, Rezende RM, Butovsky O, Lassmann H, Weiner HL (2018) Acute microglia ablation
27 induces neurodegeneration in the somatosensory system. Nat Commun 9:4578.

28 Santos VR, Pun RYK, Arafa SR, LaSarge CL, Rowley S, Khademi S, Bouley T, Holland KD, Garcia-Cairasco N,
29 Danzer SC (2017) PTEN deletion increases hippocampal granule cell excitability in male and
30 female mice. Neurobiol Dis 108:339-351.

31 Sarn N, Thacker S, Lee H, Eng C (2021a) Germline nuclear-predominant Pten murine model exhibits
32 impaired social and perseverative behavior, microglial activation, and increased oxytocinergic
33 activity. Mol Autism 12:41.

34 Sarn N, Jaini R, Thacker S, Lee H, Dutta R, Eng C (2021b) Cytoplasmic-predominant Pten increases
35 microglial activation and synaptic pruning in a murine model with autism-like phenotype. Mol
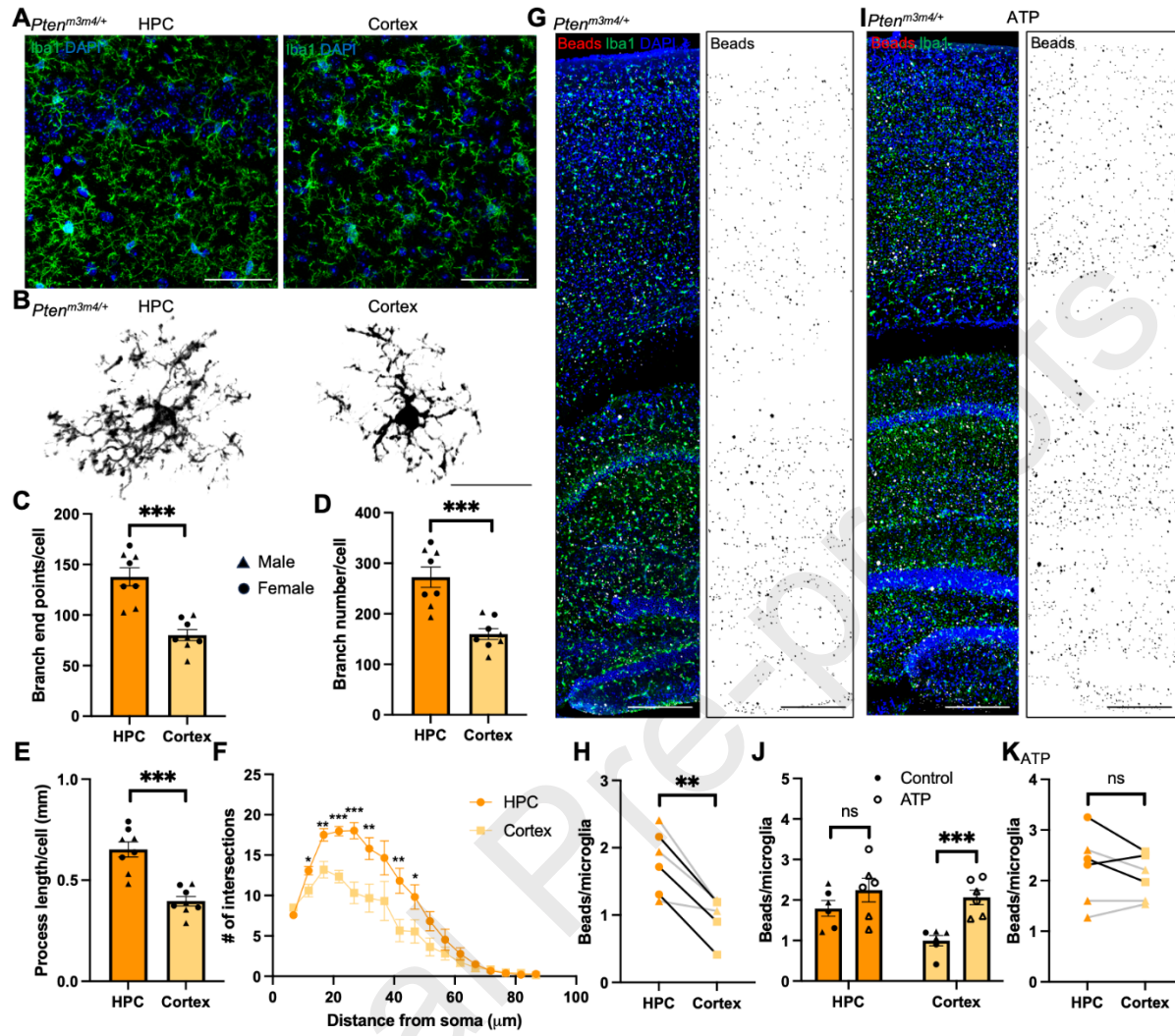36 Psychiatry 26:1458-1471.

1   Shao DD, Achkar CM, Lai A, Srivastava S, Doan RN, Rodan LH, Chen AY, Brain Development Study G,
2   Poduri A, Yang E, Walsh CA (2020) Polymicrogyria is Associated With Pathogenic Variants in
3   PTEN. Ann Neurol 88:1153-1164.

4   Streit WJ, Walter SA, Pennell NA (1999) Reactive microgliosis. Prog Neurobiol 57:563-581.

5   Sun D, Tan ZB, Sun XD, Liu ZP, Chen WB, Milibari L, Ren X, Yao LL, Lee D, Shen C, Pan JX, Huang ZH, Mei L,
6   Xiong WC (2021) Hippocampal astrocytic neogenin regulating glutamate uptake, a critical
7   pathway for preventing epileptic response. Proc Natl Acad Sci U S A 118.

8   Tan YL, Yuan Y, Tian L (2020) Microglial regional heterogeneity and its role in the brain. Mol Psychiatry
9   25:351-367.

10 Tan Z, Robinson HL, Yin DM, Liu Y, Liu F, Wang H, Lin TW, Xing G, Gan L, Xiong WC, Mei L (2018) Dynamic
11   ErbB4 Activity in Hippocampal-Prefrontal Synchrony and Top-Down Attention in Rodents.
12   Neuron 98:380-393.e384.

13 Tariq K, Cullen E, Getz SA, Conching AKS, Goyette AR, Prina ML, Wang W, Li M, Weston MC, Luikart BW
14   (2022) Disruption of mTORC1 rescues neuronal overgrowth and synapse function dysregulated
15   by Pten loss. Cell Rep 41:111574.

16 Tilot AK, Bebek G, Niazi F, Altemus JB, Romigh T, Frazier TW, Eng C (2016) Neural transcriptome of
17   constitutional Pten dysfunction in mice and its relevance to human idiopathic autism spectrum
18   disorder. Mol Psychiatry 21:118-125.

19 Tilot AK, Gaugler MK, Yu Q, Romigh T, Yu W, Miller RH, Frazier TW, 2nd, Eng C (2014) Germline
20   disruption of Pten localization causes enhanced sex-dependent social motivation and increased
21   glial production. Hum Mol Genet 23:3212-3227.

22 Umpierre AD, Wu LJ (2021) How microglia sense and regulate neuronal activity. Glia 69:1637-1653.

23 Vidal-Itriago A, Radford RAW, Aramideh JA, Maurel C, Scherer NM, Don EK, Lee A, Chung RS, Graeber
24   MB, Morsch M (2022) Microglia morphophysiological diversity and its implications for the CNS.
25   Front Immunol 13:997786.

26 Villa A, Gelosa P, Castiglioni L, Cimino M, Rizzi N, Pepe G, Lolli F, Marcello E, Sironi L, Vegeto E, Maggi A
27   (2018) Sex-Specific Features of Microglia from Adult Mice. Cell Rep 23:3501-3511.

28 Vinet J, Weering HR, Heinrich A, Kalin RE, Wegner A, Brouwer N, Heppner FL, Rooijen N, Boddeke HW,
29   Biber K (2012) Neuroprotective function for ramified microglia in hippocampal excitotoxicity. J
30   Neuroinflammation 9:27.

31 Vogt D, Cho KKA, Lee AT, Sohal VS, Rubenstein JLR (2015) The parvalbumin/somatostatin ratio is
32   increased in Pten mutant mice and by human PTEN ASD alleles. Cell Rep 11:944-956.

33 Winden KD, Ebrahimi-Fakhari D, Sahin M (2018) Abnormal mTOR Activation in Autism. Annu Rev
34   Neurosci 41:1-23.

1 Wolf SA, Boddeke HW, Kettenmann H (2017) Microglia in Physiology and Disease. Annu Rev Physiol
2   79:619-643.

3 Wu W, Li Y, Wei Y, Bosco DB, Xie M, Zhao MG, Richardson JR, Wu LJ (2020) Microglial depletion
4   aggravates the severity of acute and chronic seizures in mice. Brain Behav Immun 89:245-255.

5 Yehia L, Keel E, Eng C (2020) The Clinical Spectrum of PTEN Mutations. Annu Rev Med 71:103-116.

6 Zhao S, Umpierre AD, Wu LJ (2024) Tuning neural circuits and behaviors by microglia in the adult brain.
7   Trends Neurosci.

8 Zhou X, Wei J, Li L, Shu Z, You L, Liu Y, Zhao R, Yao J, Wang J, Luo M, Shu Y, Yuan K, Qi H (2022) Microglial
9   Pten safeguards postnatal integrity of the cortex and sociability. Front Immunol 13:1059364.

10

11 • Microglia in the hippocampus are morphologically more complex than in the cortex.
12 • Phagocytic capacity of hippocampal microglia is higher than cortical microglia.
13 • *Pten^{m3m4}* increases morphological complexity and phagocytic capacity of microglia.
14 • Microglia correct *Pten^{m3m4}* induced overexcitation of the hippocampus but not cortex.
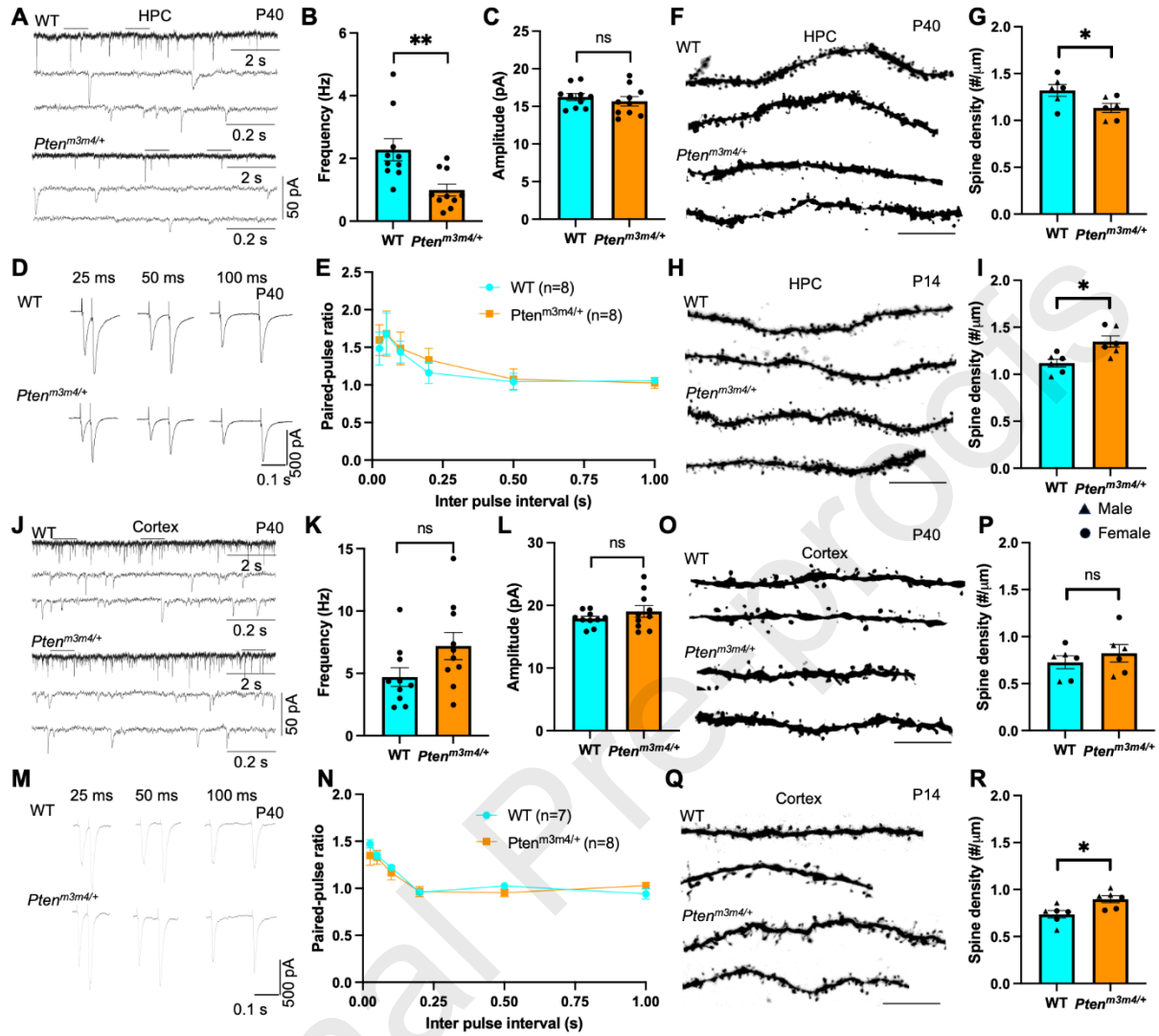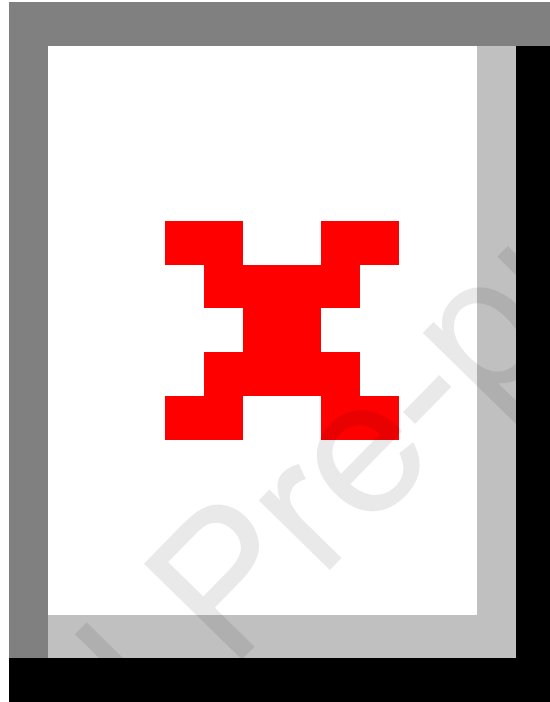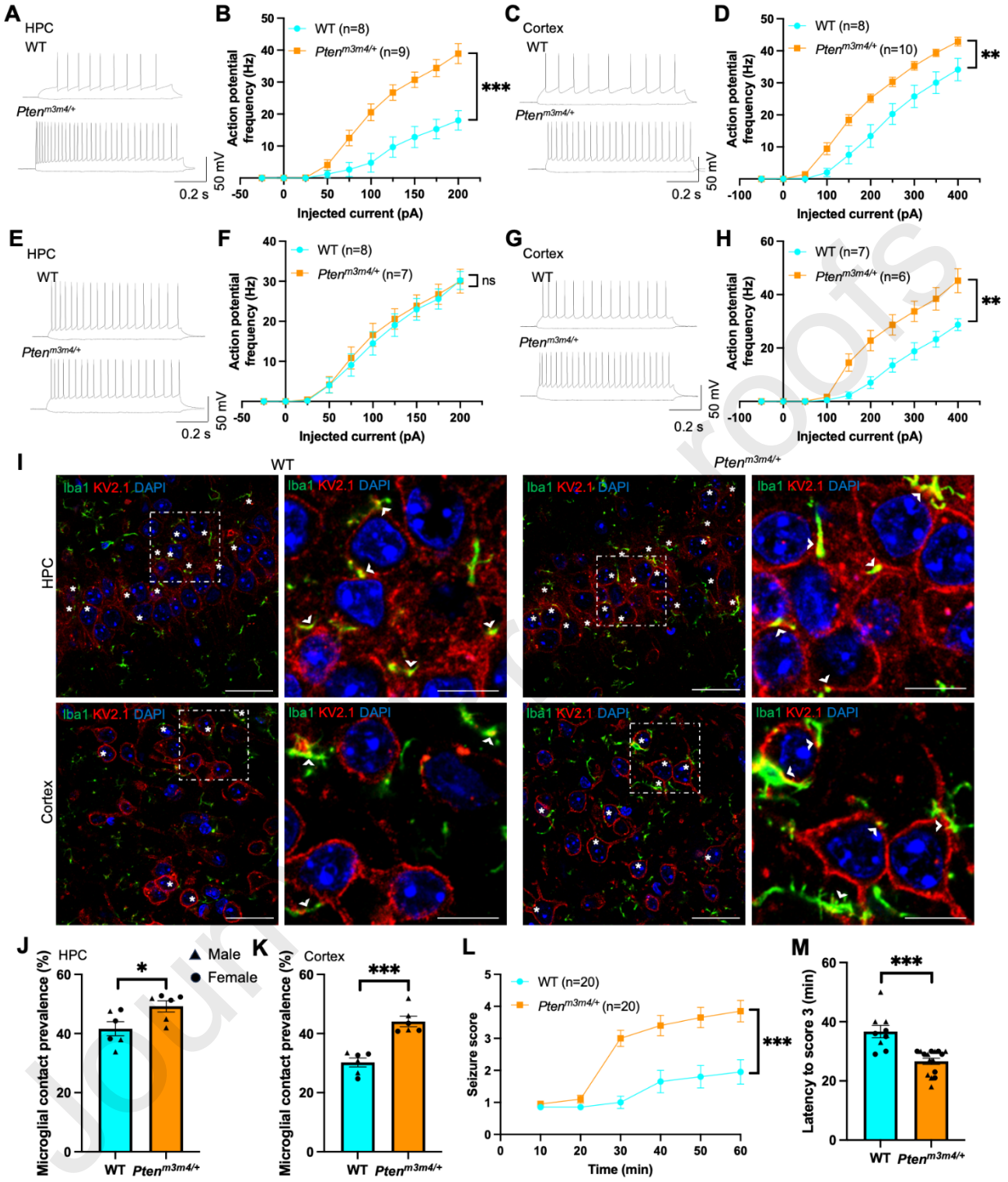15 • Microglia protect *Pten^{m3m4/+}* mice from developing spontaneous seizure.

16

1

25

1

1

1

1